From Structure to Function: From the Development of a Curved Hetero-Oligomer to the Development of an Actuated Glucose Sensor

by

Christopher W. Morgan

B.S. Chemistry, Duquesne University, 2004

Submitted to the Graduate Faculty of

The University of Pittsburgh in partial fulfillment

of the requirements for the degree of

Masters in Science of Organic Chemistry

University of Pittsburgh
2007

UNIVERSITY OF PITTSBURGH

Department of Chemistry

This thesis was presented

by

Christopher W. Morgan

It was defended on

December 6, 2006

and approved by

Dr. Dennis Curran

Dr. Craig Wilcox

Thesis Director: Dr. Christian Schafmeister

From Structure to Function: From the Development of a Curved-Hetero-Oligomer to the Development of an Actuated Glucose Sensor

Christopher W. Morgan, M.S.

University of Pittsburgh, 2007

The Schafmeister research group has developed a technology for synthesizing bis-peptide oligomers that adopt well defined structure dependent upon the rich stereochemistry of the independent bis-amino acid monomers used in its construction. These bis-amino acid monomers are designed to construct rigid bis-peptide scaffolds by utilizing a pair of amide bonds that form a 2,5 diketopiperazine (DKP) ring linkage between two monomers. It is hoped to be able to precisely position functionality within our rigid scaffolds so as to allow us to explore potential applications with our bis-peptide oligomers. Developing new bis-amino acid monomers will help achieve this goal. The first part of this thesis outlines the synthesis of the *pip5(2R5R)* and *pip5(2R5S)* bis-amino acid monomers. The newly synthesized *pip5(2R5S)* monomer was then coupled into a bis-peptide sequence with the previously synthesized *pip5(2S5R)* monomer. Molecular modeling predicted that this particular sequence formed a tight turn in space; a useful structural motif for the exploration of small cavities and clefts. The solution structure of this bis-peptide oligomer was determined by 2D-NMR techniques including a ROESY to determine important close contact information between protons on the same monomer and protons on adjacent monomers. In addition, two powerful 2D-NMR techniques that have begun their integration into our lab for structure determination were used to provide more NMR restraints on the bis-peptide structural model. These included amplitude-constrained multiplet evaluation of $^{3}J_{HH}$ coupling constants and the use of residual dipolar coupling (RDC) constants. Lastly, I have recently begun work on synthesizing a glucose sensitive

molecular actuator. This molecular actuator is a water-soluble rod-hinge-rod motif that converts from its disordered "open" form to an ordered "closed" form upon reversible binding to glucose through the 4,6 and 1,2 diol pairs. It is envisioned that these rod-hinge-rod motifs can eventually be used for potential applications such as nanovalves.

TABLE OF CONTENTS

LIST OF TABLES

LIST OF FIGURES

LIST OF SCHEMES

List of Abbreviations

Boc	*tert*-Butoxycarbonyl
Boc_2O	Di-*tert*-butyl dicarbonate
Cbz	Carboxybenzyl
DCC	Dicyclohexylcarbodiimide
DCM	Dichloromethane
DIPEA	*N,N*-Diisoproylethylamine
DKP	Diketopiperazine
DMAP	4-Methyldiaminopyridine
DMF	*N,N*-Dimethylformamide
EDT	Ethane dithiol
EtOAc	Ethyl acetate
Fmoc	*9*-Fluorenylmethoxycarbonyl
HATU	*O*-(7-azabenzotriazol-1-yl)-*N,N,N',N'*-tetramethyluronium hexafluorophosphate
HMBC	Heteronuclear multiple bond correlation spectroscopy
HMQC	Heteronuclear multiple quantum coherence
HPLC	High performance liquid chromatography
MeCN	Acetonitrile
MeIm	Methylimidazole
MeOH	Methyl alcohol
MS	Mass spectrometry
MSNT	1-(mesitylene-2-sulfonyl)-3-nitro-1,2,4-triazole
NHS	*N*-hydroxy succinimide
NOESY	Nuclear Overhauser enhancement spectroscopy
ROESY	Rotating frame Overhauser enhancement spectroscopy
TFA	Trifluoroacetic acid
TFMSA	Trifluoromethanesulfonic acid
TFP	2,2,3,3-tetrafluoropropyl
THF	Tetrahydrofuran
TIPS	Triisopropylsilane

PREFACE

Reaching this point in my career has been accomplished with persistent dedication and drive. However, the help and support of many influential individuals has been equally as important. It is at this time that I would like to acknowledge and thank all the individuals that have helped me reach my goal. Their influence not only allowed me to complete my degree, but it will continue to guide and aid me throughout my entire career.

I owe a great deal of thanks to my advisor Christian Schafmeister for his constant encouragement and guidance in all aspects of my research. I was blessed with an outstanding advisor devoted to pushing me to achieve great things. With his help I have undoubtedly become a better chemist and scientist. This will most definitely help propel my career forward after graduate school. In addition to my advisor, the entire Schafmeister group has provided great support during my time at the University of Pittsburgh. No group member will be forgotten.

I also owe a special thanks to my friends and family. They have all stuck by my side through the good and bad times. Without their love and support, achieving this high point in my life would not be as rewarding. The one person I owe a great deal of thanks to is my fiancée, Valerie. She has kept by my side and has provided constant motivation as well as encouragement. Words cannot express my love and respect for her. She has helped me through

the endless obstacles that I faced alone and those that we face together. On July 7, 2007 Valerie and I will wed and start the rest of our lives together. This could not happen at a more perfect time in my life. I promise her that I will always strive to do great things but to also keep her and my family first. Without them my success in life means nothing to me.

1.0 INTRODUCTION AND BACKGROUND

1.1 INTRODUCTION TO MY WORK

Over the last decade there has been a rapidly emerging field of science encompassing a wide area of interests including medicine, physics, engineering, biology, and chemistry.[1] This revolutionary field of nanotechnology has and will spur continual advances in our current technology which includes computer technology, medical diagnostic equipment, high-performance robotics, and maybe even energy independence from major industrial nations.[1] There still remains tremendous amount of progress to be made, but moderate advances have given keen insight into the world that can revolve around such a technology.

Nanotechnology is defined by the National Nanotechnology Initiative website[2] as "the understanding and control of matter at dimensions of roughly 1 to 100 nanometers, where unique phenomena enable novel applications." At this particular "nano-scale regime", the fundamental properties of materials tend to differ from their particular properties at the atomic level or the bulk material.

It is the goal of nanotechnology to learn how to harness these characteristic properties so as to create molecules with unique chemical, physical, and biological functions. In order to accomplish this task it becomes necessary to control the architecture of these nano-scale molecules. But how does one create functional molecules while controlling the exact structure to

be within the "nano-scale regime"? In the realm of materials science, many groups are continuing to work on this task of synthesizing and assembling small molecules with certain function or characteristics ultimately creating molecular devices and machines. Solving these aforementioned problems has led to the development of many new areas of chemistry as well as unique approaches for constructing important macromolecules. A small selection of these approaches will be summarized here.

1.2 SUPRAMOLECULAR CHEMISTRY-MOLECULAR RECOGNITION AND SENSING

Supramolecular chemistry offers a way of creating macromolecules that avoids the complications of chemical synthesis. Supramolecular chemistry is a discipline that utilizes reversible interactions such as hydrogen bonding, electrostatic interactions, π- π interactions, metal coordination, hydrophobic forces, and van der Walls forces instead of covalent bonding. Areas explored by this discipline include host-guest chemistry, self-assembly, and molecular recognition.

One of the earlier goals of supramolecular chemistry was to selectively complex cationic species. Professor Jean-Marie Lehn has helped to pioneer this field and has continued to add interesting examples of dynamic devices. Lehn and co-workers[3] have developed an assembly of ion-regulated substrate binders. These pyridine triads exist in a "W-shaped" conformation that undergoes a switching mechanism to a "U-shaped" cavity upon the addition Zn(II) cations. These Zn(II) cations facilitate the receptor to act as a molecular tweezer that binds to a 1,10-phenantholine substrate (Figure 1).

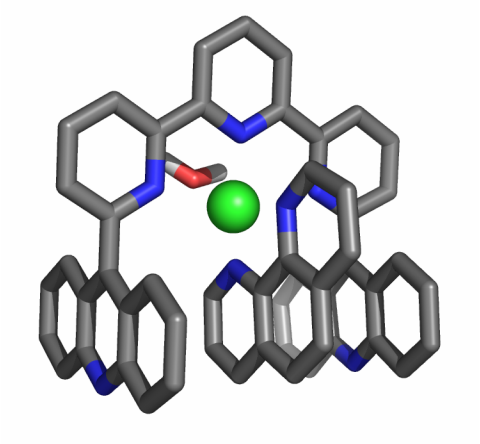

Figure 1 (adapted from ref [3]): Representation of the pyridine triad in the "W-shaped" conformation in the presence of Zn(II) bound to a 1,10 phenantholine substrate molecule.[3]

They also synthesized an analogous system containing a central pyrimidine ring.[3] This particular receptor is initially in the "U-shaped" conformation for substrate binding. Upon addition of Cu(I), the "U-shaped" conformation of the receptor is disrupted and converted into the "W-shaped" conformation that is incapable of binding an electron acceptor.

Jeppesen, Sessler and co-workers[4] have also utilized reversible molecular recognition via addition of ions. This supramolecular host system is a tetra-tetrathiafulvalene calix[4]pyrrole that acts as a receptor for neutral electron acceptors such as tetrafluoro-ρ-benzoquinone forming a 1:2 complex of receptor to substrate (Figure 2). In the absence of an anion, the tetra-TTF calix[4]pyrrole exists in a 1,3-alternate conformation with two arms pointing in opposite directions that each bind a substrate molecule. However, the addition of chloride anions results in the release of the substrate as the Cl^- facilitates a conformational change to a cone structure (Figure 2).[4]

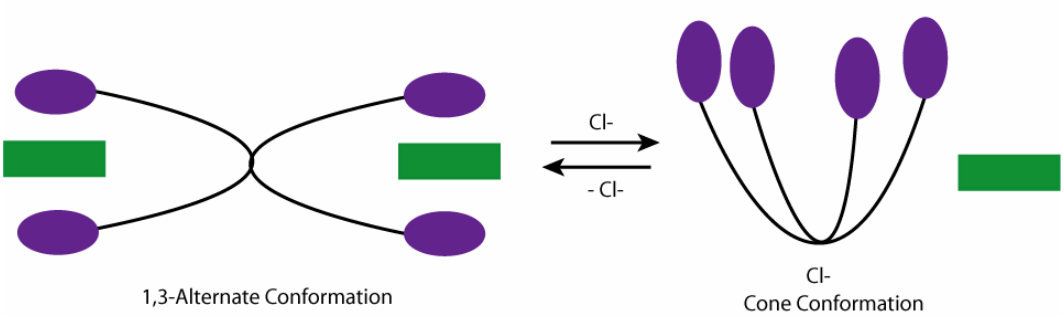

Figure 2 (adapted from ref [4]): Cartoon representation illustrating the change in conformation with the addition and removal of chloride anions to a CH_2Cl_2 solution of the tetra-TTF Calix[4]pyrrole and the electron-deficient guest tetrafluoro-ρ-benzoquinone (green rectangle).[4]

1.3 MOLECULAR DEVICES AND MACHINES

The idea of using molecular recognition via the use of weak interactions has been put to extended uses in the construction of molecular devices and molecular machines. Stoddart and co-workers may be best known for their work with catenanes and rotaxanes.[5] They have specialized in designing these movable elements to be controlled by external stimuli such as pH, electricity, and light. Recently they have developed a pH-driven supramolecular valve by utilizing the immobilization of a diaklyammonium-tethers to porous silica with dibenzo[24]crown-8 (DB24C8).[6]

This device is operated by trapping luminescent probe molecules (coumarin 460) in the diakylammonium tethered pores of the silica and capping these filled pores with DB24C8 via the formation of hydrogen bonds. Treatment with base changes the protonation state of the tethers disrupting the H-bonds and releasing the coumarin 460.[6]

Another impressive example of an assembled molecular machine has been the construction of an azobenzene-modified nanoporous membrane (Figure 3) presented by Brinker and co-workers.[7] This elegant construction utilized the properties of azobenzene to photo-convert to an extended "trans" form upon irradiation with visible light (435 nm) and to a more bent "cis" form upon irradiation with UV light (360nm). An azobenzene functionalized nanoporous membrane was mounted to an indinium tin oxide (ITO) electrode. The photoresponsive azobenzene was able to regulate the flow of ferrocene compounds to the electrode. When in the extended "trans" form the pore size is decreased and when photo-converted to the "cis" form the pore size increased thus increasing flow and increasing current at the ITO electrode.[7]

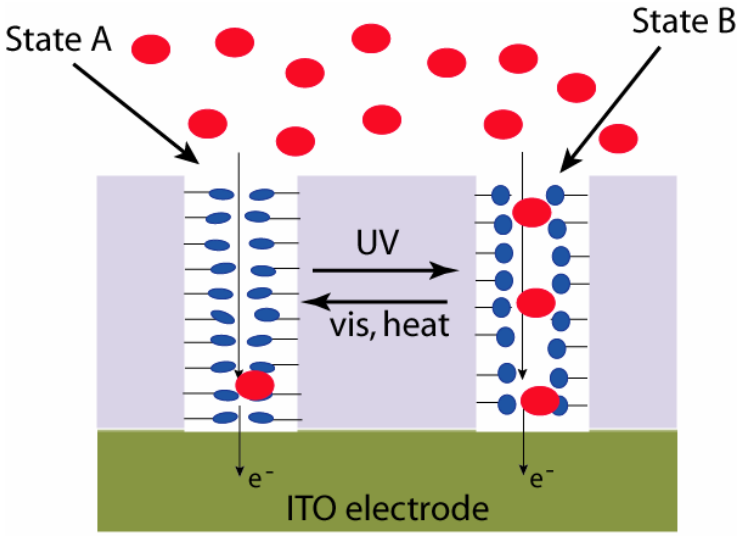

Figure 3 (adapted from ref [7]): Azobenzene functionalized pores will open in response to ultraviolet irradiation and close in response to visible light irradiation. The closed pores in state A slow the flow of electrochemically active ferrocenes (red circles) to the ITO electrode. The open pores in state B allow higher transport to the electrodes and result in a measurable current at the ITO electrode.[7]

1.4 MODULAR APPROACH TO NANO-SCALE MOLECULES

A brief look into nature immediately tells us that it is capable of creating functional macromolecules that carry out critical life functions in our bodies ranging from catalysis, to self replication, to molecular transportation. Nature has done this by utilizing amino acids and nucleotides as monomers (building blocks) to create elegant proteins with a predetermined function as well as DNA and RNA that make life possible. These impressive macromolecules are able to fold into precise secondary, tertiary, and quaternary structure by utilizing a network of specific interactions. In a way to mimic the actions of nature, many groups have developed a modular approach of covalently linking together small monomers that collectively assemble a functional macromolecule. In addition to solely modular synthesis, some groups have utilized the presence of secondary interactions to stabilize certain secondary structures in ways analogous to proteins thus generating certain architectures.

A number of groups are attempting to synthesize specific architectures by utilizing designer dendrimers. Another approach developed by Michl[8] and co-workers utilizes a "Tinkertoy" construction set of trigonal and tetragonal connectors with metal-ligating termini that can piece together to create large macromolecules with certain functions.

A large collection of modular approaches to macromolecule design fall under the heading of foldamers. A foldamer is a discrete chain molecule or oligomer that adopts secondary structure stabilized by non-covalent interactions such as hydrogen-bonding. These artificial molecules are capable of forming helices and β-sheets and have found uses in self-assembly, molecular recognition, and host-guest chemistry.

Moore and co-workers have developed shape-persistent molecules[9,10] by connecting phenylene-ethynylene monomers as building blocks. With this modular approach they have developed new functionalized monomers that are able to create macrocycles (Figure 4) with defined non-polar or slightly polar cavities.[9,10] More recently, Moore and co-workers[11] have developed helical structures that contain functionalized inner cavities by using a N,N-(dimethylamino)pyridine monomer which directs its pyridine nitrogen into the inner cavity (Figure 5).

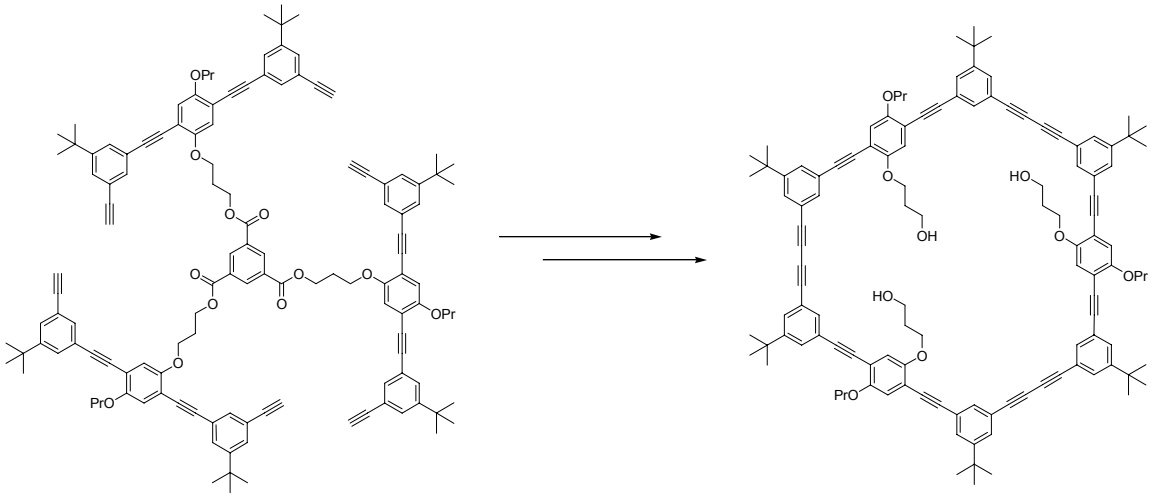

Figure 4 (adapted from ref [10]): Representative template directed synthesis of phenylene-ethynylene macrocycle.

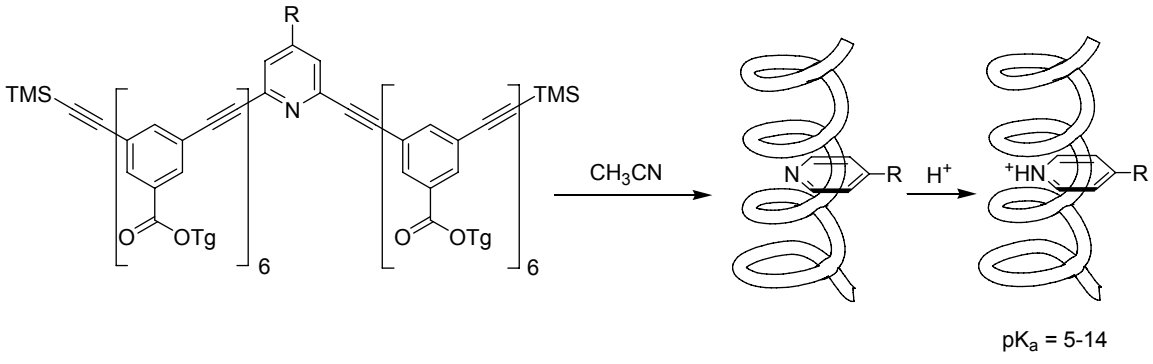

Figure 5 (adapted from ref [11]): Schematic representation of functionalized helical cavities.

Another leader in foldamer development is Samuel Gellman with the creation of his β-peptides. Since first discovering in 1999[12] that hexa-β-peptides composed of trans-2-aminocyclohexanecarboxlyic acid (ACHC) adopt a 14-helix conformation in water, Gellman and co-workers have successfully developed β-sheets[13] as well as hairpin turns.[14] In addition this group has successfully synthesized β-peptide inhibitors of human cytomegalovirus entry.[15]

Gellman's β-peptide foldamers represent a promising approach to the task of synthesizing macromolecules with the ability to synthesize many oligomers with a few β-amino acids. However, the ability to accurately predict the exact folding properties of these relatively short oligomers severely limits the capacity of this technique when attempting to create larger and more intricate macromolecules.

1.5 SCHAFMEISTER APPROACH TO DESIGNER NANOSCALE MACROMOLECULES

This problem of predicting folding properties has been ongoing in the area of producing unnatural proteins. However, significant progress has been made in this area of de novo design[17,18], but the protein folding problem is far from being resolved in the production of unnatural proteins. It is this idea of bypassing these folding problems that has spurred a revolutionary design of bis-amino acid oligomers that adopt well defined structure dependent upon the rich stereochemistry of the independent bis-amino acid monomers used in its construction. By eliminating the problem of predicting complex folding patterns, it is envisioned that we will be capable of producing large macromolecules with precisely defined structure and functionality.

These bis-amino acid monomers (Figure 6) are designed to construct rigid scaffolds by utilizing a pair of amide bonds that form a 2,5 diketopiperazine (DKP) ring linkage between two monomers. The overall structure of a chosen oligomer is dependent upon the exact stereochemistry of each bis-amino acid monomer, the order of sequence of the monomers, and the inherent nature of the monomer to adopt a particular ring conformation.

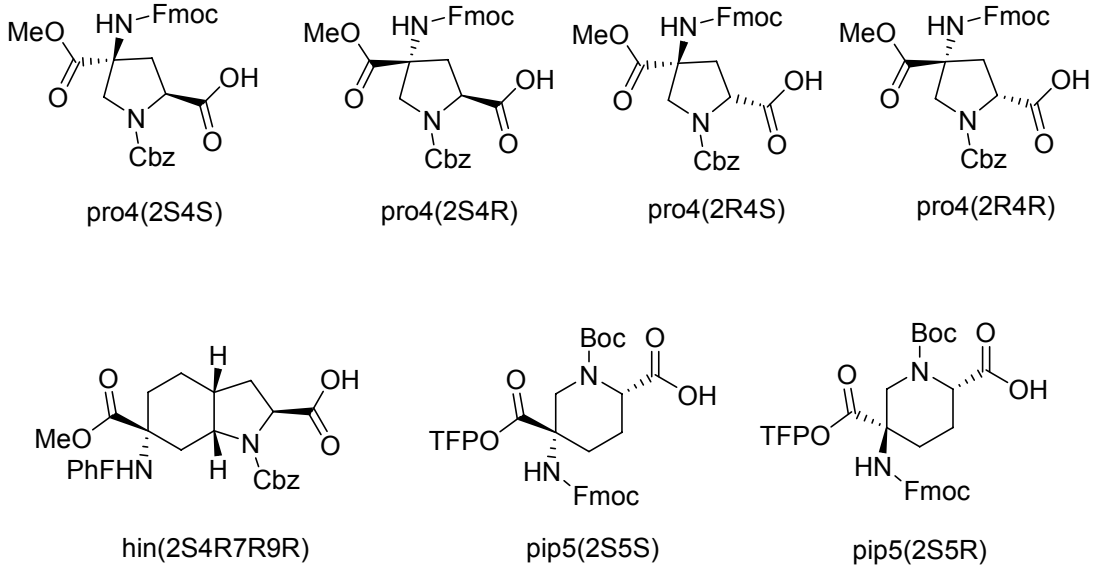

Figure 6: Bis-amino acid monomers synthesized to date in our lab.

There has been several structural characterization studies[19-22] performed on homo- and hetero-oligomers synthesized with these monomers, and it is our hope to be to able to rationally design and predict the exact architecture of any oligomer synthesized based upon the information we learn in structural studies.

We wish to ultimately be able to create large cavities and clefts similar to those described previously without the need of external stimuli to induce binding. The research project presented here begins with the task of synthesizing the *pip5(2R5R)* and *pip5(2R5S)* bis-amino acid monomers. The newly synthesized *pip5(2R5S)* and the previously synthesized *pip5(2S5R)* monomers were used in the construction of a curved hetero-oligomer in order to gain more

insight into bis-peptide sequences that are capable of forming cavities and clefts. The structural characterization of this particular bis-peptide sequence led to the use of two structural elucidation techniques that have recently begun their integration in our lab. These techniques will aid our structural studies as well as help demonstrate our ability to rationally design architectures. These techniques include the use of amplitude-constrained multiplet evaluation for $^{3}J_{HH}$ coupling constants, and the use of residual dipolar coupling to determine the molecular conformation or shape of a molecule by relating two distant ends or parts of the molecule.

The structural development of useful bis-peptide oligomers lays a foundation upon which we can create useful and functional macromolecules. The future of our group is in the development of useful applications with these architecturally designed macromolecules. Therefore, the latter part of this document details the development of a potential application opens a gateway to constructing important nano-scale devices.

One such device is the construction of a molecularly actuated glucose sensor that consists of a rod-hinge-rod motif. These actuators possess a controlled mechanism that can reversibly switch between a disordered "open" form and an ordered "closed" form through the reversible binding to glucose. Such a device can lead to the development of our own nanopore channels. By functionalizing nanoporous membranes with these molecular actuators we can form nano-scale valves (Figure 7) that control the transport of insulin.

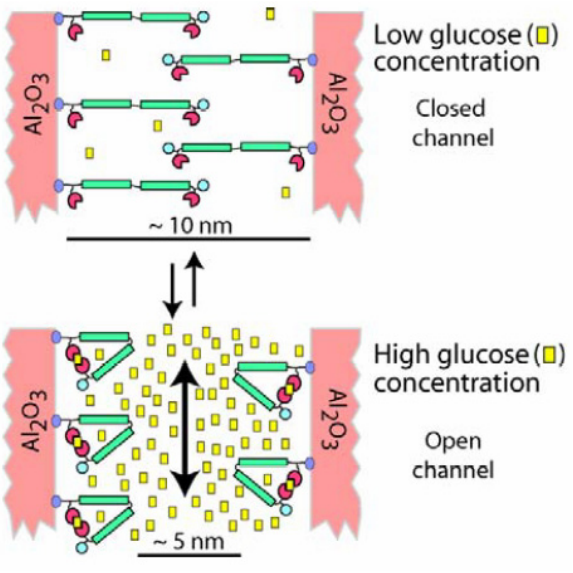

Figure 7: Molecular valves formed by attaching glucose sensitive molecular actuators to the insides of ~ 10 nanometer diameter alumina channels. At low glucose (yellow) concentrations the actuators will be disordered and block the channel ("valveclosed" state). In the presence of high glucose concentrations, the actuators will fold back, creating a channel with a diameter of about 5 nanometers, large enough to allow small proteins such as insulin to pass through ("valve-open" state).

2.0 SYNTHESIS OF PIPECOLIC ACID MONOMERS AND SECOND GENERATION PYRROLIDINE ACID MONOMERS

2.1 SYNTHESIS OF *PIP5(2R5R)* AND *PIP5(2R5S)* MONOMERS

As discussed in the previous chapter, our goal is to create macromolecules with defined tertiary structure. Our approach utilizes the assembly of cyclic bis-amino acid monomers that are coupled through two pairs of amide bonds forming 2,5 diketopiperazine ring linkages. These rigid ladder-type molecules create uniquely defined structures based on the rich stereochemistry of each individual monomer. Achieving more control over structural design is dependent on the number and types of bis-amino acid monomers in our "molecular tool box". For an oligomer containing N number of monomers (using our 7 different monomers), the total number of possible combinations is 7^N. In our lab 7 monomers had been developed and utilized in the design of oligomers and hetero-oligomers. The synthesis of *pip5(2R5R)* and *pip5(2R5S)* monomers will further enhance and diversify the tool box available for macromolecule synthesis.

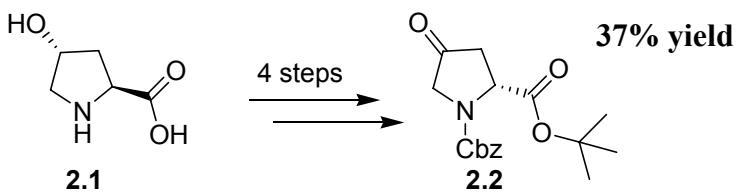

2.1 **2.2**

Scheme 1: Ketone 2.2 is synthesized in four easy steps from *trans*-4-hydroxy-L-proline with a yield of 37%.

The synthesis of these particular monomers is straight forward as it parallels that of their previously developed monomers.[23] Ketone **2.2**[20] (Scheme 1) was synthesized from readily available, inexpensive *trans*-4-hydroxy-L-proline.

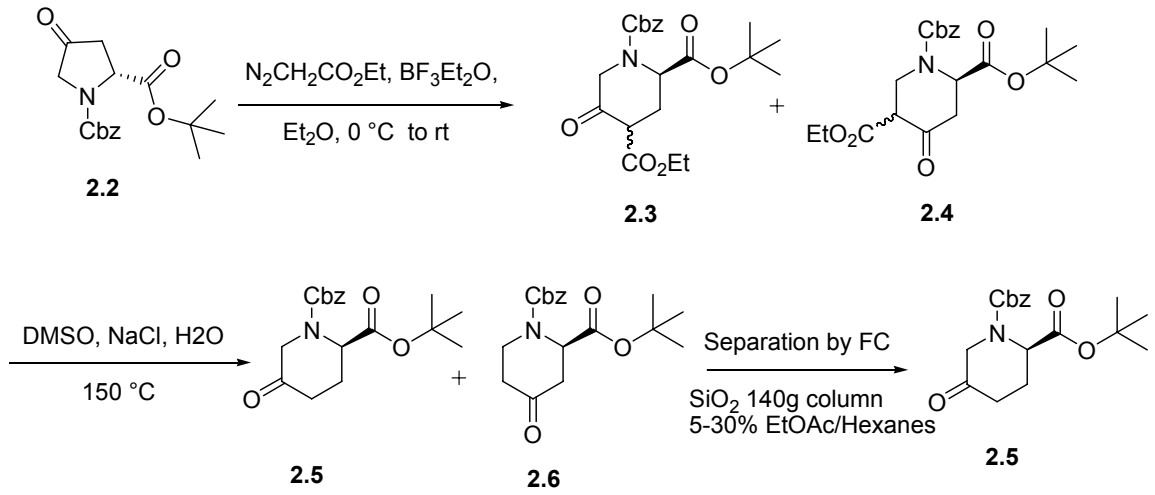

Scheme 2: Synthesis of ketone 2.5.

Compound **2.2** was subjected to a two-step cyclic ketone homologation reaction[24] (Scheme 2) yielding a mixture of two regioisomeric ketones **2.3** and **2.4**. The initial step involved a ring expansion[24] reaction with ethyl diazo acetate in the presence of the lewis acid $BF_3.Et_2O$ at 0 °C. The mixture of **2.3** and **2.4** was purified by flash chromatography on SiO_2 gel with a 5-30% EtOAc in hexanes gradient to remove colored impurities before performing a Krapcho decarbethoxylation[25] generating a mixture of **2.5** and **2.6**. These two regioisomeric ketones were separated by flash chromatography on SiO_2 gel with a 5-30% EtOAc in hexanes gradient. Ketone **2.5** is the desired intermediate for both *pip5(2R5R)* and *pip5(2R5S)* monomers and was identified by comparing the ^1H NMR spectra of its enantiomer that was previously synthesized in our lab.[23]

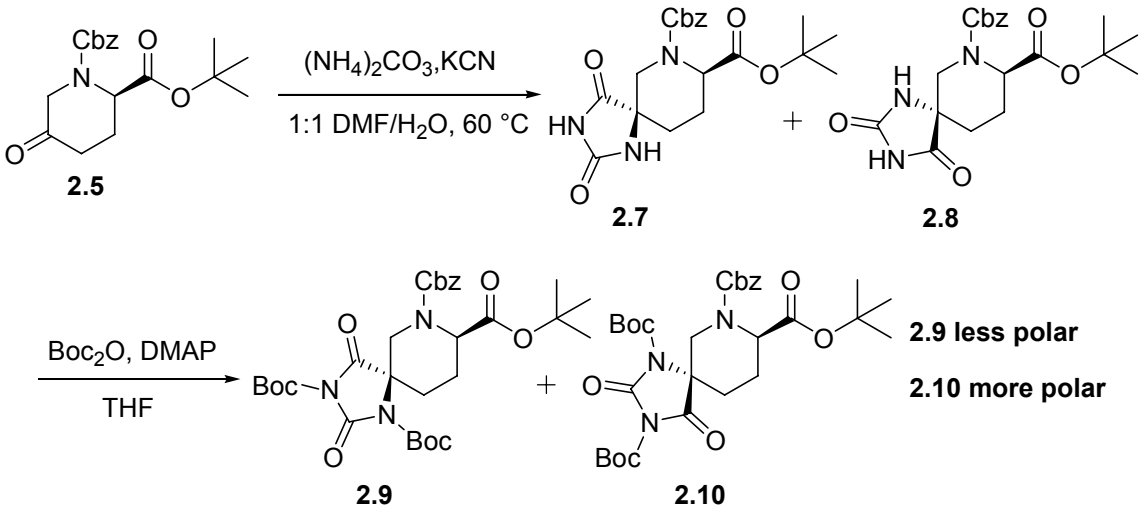

Scheme 3: Synthesis of bis-Boc protected hydantoins 2.9 and 2.10.

Ketone **2.5** next underwent the Bucherer-Bergs reaction[26] (Scheme 3) in order to create a quaternary stereocenter that can be eventually converted to the second amino acid. Hydantoins **2.7** and **2.8** were generated in a 3:2 ratio determined by ^{1}H NMR of the crude mixture. Unfortunately, these hydantoins are inseparable by SiO_2 gel chromatography[23]. It is necessary to bis-Boc protect **2.7** and **2.8** to form **2.9** and **2.10** which are separable by SiO_2 gel chromatography. These bis-Boc protected hydantoins were separated by flash chromatography on SiO_2 gel with a 5-30% EtOAc in hexanes gradient.

2.2 STEREOCHEMICAL ASSIGNMENT OF BIS-BOC PROTECTED HYDANTOINS

In order to verify the stereochemistry of **2.9** and **2.10**, the Boc groups must be removed so as to be able to observe NOE interactions between the amide hydrogen and diastereotopic hydrogens on the six-membered ring. Boc protecting groups of **2.9** and **2.10** were removed with exposure

to a 3:7 mixture of TFA in DCM for 3 hours with stirring (Scheme 4). The *tert*-butyl protecting group is also labile to these conditions and was removed, yielding deprotected hydantoins **2.11** and **2.12**.

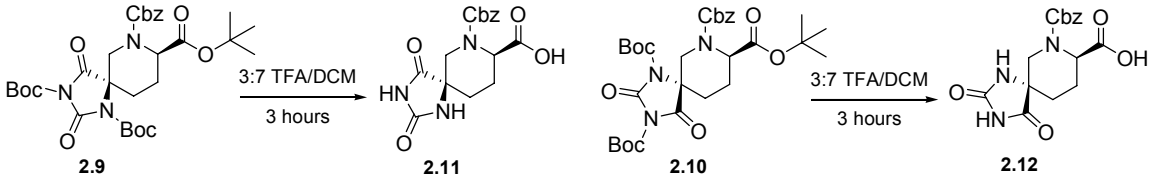

Scheme 4: Deprotection of bis-Boc protected hydantoins to 2.11 and 2.12.

2D COSY and 2D ROESY experiments were performed for compounds **2.11** and **2.12** in DMSO on a 500 MHz NMR in order to assign individual hydrogen resonances and to measure important NOE interactions (Figure 8). ROESY analysis revealed correlations between amide hydrogen H1 with H6α and H10α but not 9α for **2.11**. Hydantoin **2.12** gives rise to ROESY correlations between amide H1 with H6β, H9β, and H10β.

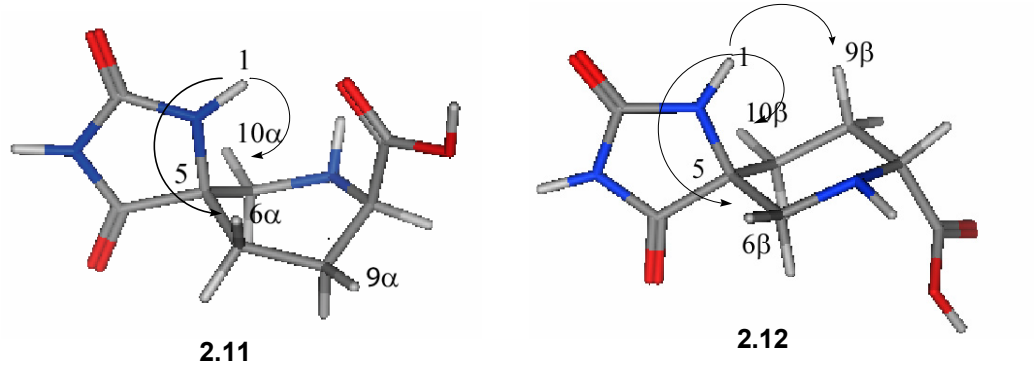

Figure 8: Lowest energy conformations of 2.11 and 2.12 determined *in vacuo* by carrying out a stochastic search[27] with an MMFF94x forcefield using molecular mechanics package MOE.[28]

The molecular mechanics package MOE[28] was used to carry out a stochastic conformational search[27] of hydantoins **2.11** and **2.12** in order to locate the lowest MMFF94x[29-32] energy minima *in vacuo* (Figure 8). The modeled structures of the global energy minimum for both **2.11** and **2.12** are in strong agreement with their observed ROESY correlations. In addition,

the observed correlations are in exact agreement with the previously developed *pip5(2S5S)* and *pip5(2S5R)* monomers[23] thus absolutely determining the stereochemical assignment of bis-Boc protected hydantoins **2.9** and **2.10**.

2.3 FINISHED SYNTHESIS OF *PIP5(2R5R)* AND *PIP5(2R5S)* MONOMERS

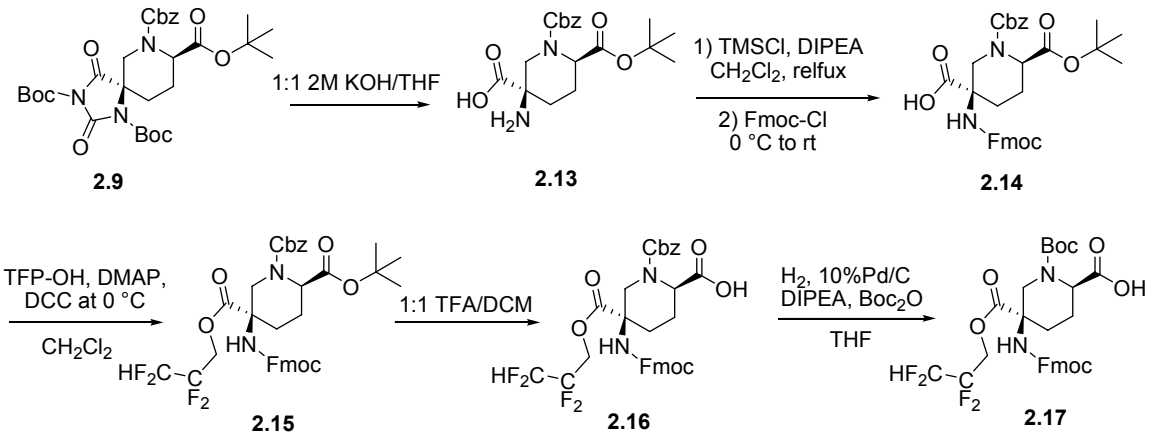

Scheme 5: Synthesis of the final pip5(2R5R) monomer, 2.17.

Bis-Boc protected hydantoin **2.9** was hydrolyzed[34] to the following amino acid **2.13** by stirring with 50% 2M KOH in THF for 45 minutes (Scheme 5). The aqueous layer was separated and cooled to 0 °C. The product was precipitated by dropwise addition of 2M HCl with pH adjustment to 6.5. Oven dried **2.13** was converted to Fmoc protected **2.14** via a two step process with TMSCl and Fmoc-Cl. Product **2.14** was purified by flash chromatography on SiO_2 gel with a 0-10% MeOH in $CHCl_3$ gradient.

Recent work in our lab[23] has demonstrated that oligomers constructed with *pip5(2S5S)* monomers that contain methyl esters undergo a base-catalyzed DKP closure at very slow rates.

Therefore, *pip5* monomers with methyl esters are not viable for oligomer synthesis. However, 2,2,3,3-tetrafluoropropyl esters have been found to be more susceptible to DKP closure under acidic conditions.[35] Therefore 2,2,3,3-tetrafluoropropyl ester versions of the *pip5(2R5R)* and *pip5(2R5S)* monomers were synthesized. Compound **2.14** was esterified with 2,2,3,3-tetrafluoropropyl alcohol in the presence of DCC and DMAP yielding a orthoganol protected **2.15**. Product **2.15** was purified by flash chromatography on SiO_2 gel with a 0-50% EtOAc in hexanes gradient. Subsequently, the *tert*-butyl protecting group was removed with 50% TFA in DCM, and the resulting deprotected product **2.16** purified by flash chromatography on SiO_2 gel with a 0-10 % MeOH in $CHCl_3$ gradient.

Finally, a one pot Cbz to Boc exchange reaction[36] was utilized transforming compound **2.16** to the orthogonally protected compound **2.17.** This final building block was purified by flash chromatography on SiO_2 gel with a 0-10% MeOH in $CHCl_3$ gradient.

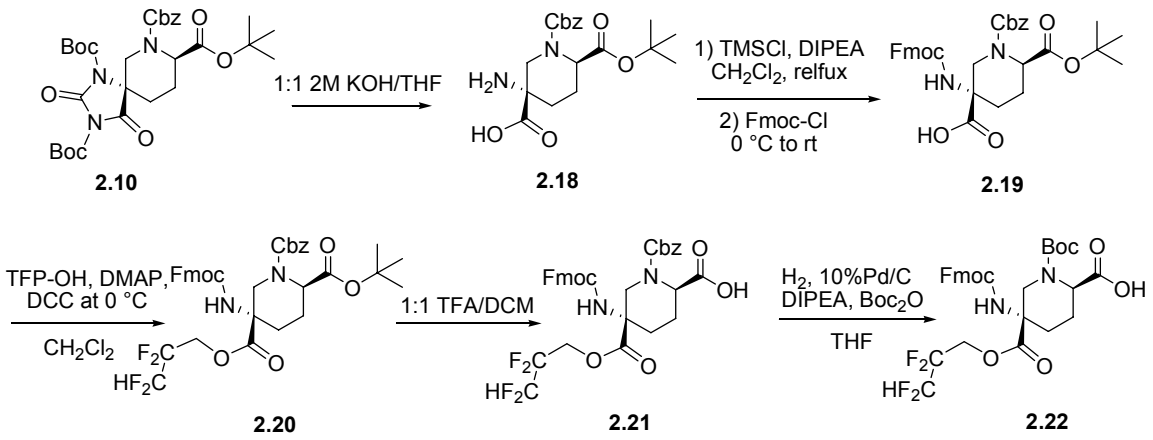

Scheme 6: Synthesis of final the *pip5(2R5S)* monomer, 2.22.

An identical strategy to Scheme 5 was followed in the production of the diastereomer *pip5(2R5S)* (**2.22**). Scheme 6 outlines the synthesis of orthoganally protected **2.22,** which was

subsequentally purified flash chromatography on SiO_2 gel with a 0-10% MeOH in $CHCl_3$ gradient.

2.4 SYNTHESIS OF 2ND GENERATION *PRO4(2R4R)* MONOMER (TFP VERSION)

In the construction of hetero-oligomers containing *pip5* monomers and *pro4* monomers it is important to have identical leaving groups in the aminolysis reactions of the DKP closure. When a *pip5(2S5S)* monomer is coupled to the N-terminus of a *pro4(2S4S)* monomer, the DKP closure between these two monomers is a very slow process.[35] Therefore, the construction of *pro4(2R4R)* 2,2,3,3-tetrafluorpropyl ester generation monomers (Scheme 7) has been undertaken for the incorporation of these monomers into hetero-oligomers with *pip5(2S5S), pip5(2S5R), pip5(2R5R),* and *pip5(2R5S)* monomers.

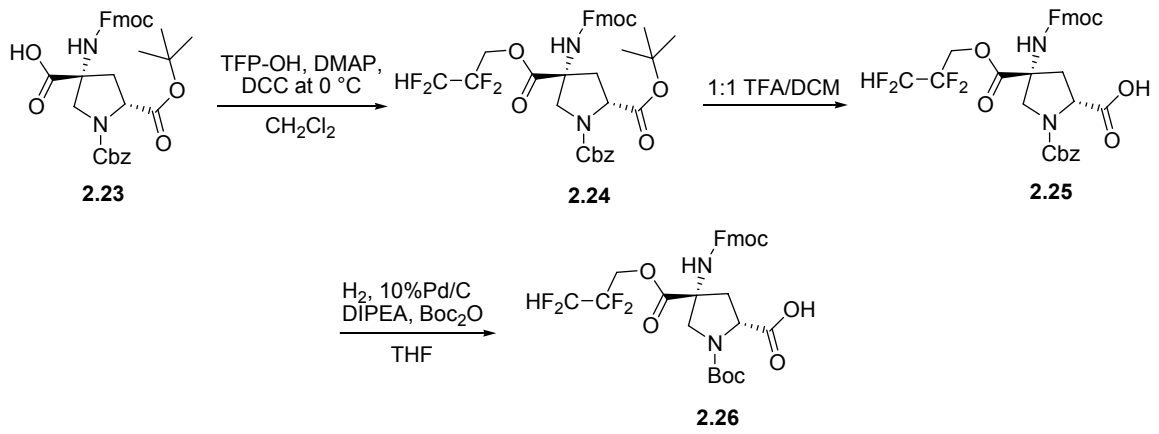

Scheme 7: Synthesis of the *pro4(2R4R)* TFP ester generation monomer, 2.26.

Intermediate **2.23**[20] was esterified to **2.24** with 2,2,3,3-tetrafluoropropyl alcohol in the presence of DCC and DMAP yielding fully, orthogonally protected **2.24**. Product **2.24** was

immediately purified by flash chromatography on SiO_2 gel with a 0-50% EtOAc in hexanes gradient. The *tert*-butyl protecting group was removed with 50% TFA in DCM, and the resulting deprotected product **2.25** was purified by flash chromatography on SiO_2 gel with a 0-10% MeOH in $CHCl_3$ gradient. Finally, the Cbz protecting group was exchanged for a Boc group via a one pot procedure[36] yielding **2.26** which was subsequentally purified by flash chromatography on SiO_2 gel with a 0-10% MeOH in $CHCl_3$ gradient.

3.0 STRUCTURAL ELUCIDATION OF CURVED HETERO-OLIGOMER

3.1 INTRODUCTION AND BACKGROUND

As discussed in Chapter 1, one goal of our group is to construct large cavities and clefts that are capable of binding small target substrate molecules. The synthesis of curved bis-peptide oligomers will aid in achieving this goal. This chapter discusses the synthesis of one such curved hetero-oligomer that utilizes two bis-amino acid monomers that had not been used in the construction of any bis-peptide oligomer to date. These *pip5(2R5R)* and *pip5(2R5S)* monomers were used to synthesize the *pip5(2S5R)-pip5(2R5S)-pro4(2S4S)-(L)*-tyrosine hetero-oligomer with standard Fmoc-solid phase peptide synthesis on the hydroxymethyl polystyrene resin. The lowest energy conformer of oligomer **3.1** determined *in vacuo* when using the Amber94[37] forcefield shows a highly curved structure shown in Figure 9.

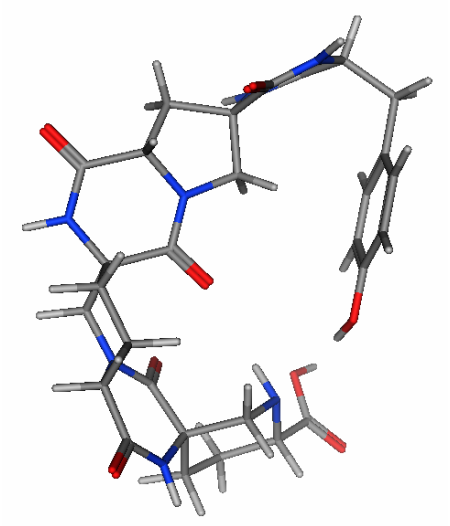

Figure 9: Lowest energy conformer of 3.1 *in vacuo* when carrying out a stochastic search[27] with an Amber94[37] forcefield using the molecular mechanics package MOE.[28]

It is this solution structure of bis-peptide **3.1** that I set to determine by using 2D-NMR experiments. I carried out a TOCSY, an HSQC and an HMBC experiment and used the data to assign every carbon and hydrogen on the molecule. I also carried out a ROESY experiment and observed several cross-peaks that indicate close contacts between hydrogen atoms within monomers as well as between monomers. In addition, two NMR techniques that our group has recently learned to use have aided in the structural determination of **3.1**. The extraction of $^{3}J_{HH}$ coupling constants from a phase sensitive COSY provided important dihedral angle information regarding the ring conformation of each monomer. Also, recently our group has demonstrated the ability to use residual dipolar coupling (RDC) constants as additional NMR restraints on our bis-peptide oligomers. RDCs restrain the angle that C-H bonds can make relative to the direction of the external magnetic field and thus relate the orientation of distant parts of an oligomer to one another to gain global information on the structure.

Residual dipolar couplings have been used extensively in the structural determination of proteins and recently have been employed in the structural assignment of small organic

molecules.[38-41] This new tool can prove to be quite a powerful technique in determining conformations of the restrained bis-peptides synthesized in our group and will be used in conjunction with *J*-coupling values and ROESY constraints to determine the solution structure of scaffold **3.1**.

3.2 MODELING THE MONOMER CONFORMATIONS WITHIN OLIGOMER 3.1

The molecular mechanics calculations performed on the sequence *pip5(2S5R)-pip5(2R5S)-pro4(2S4S)-(L)-tyrosine* (Figure 10) predicts that the pipecolic acid monomer *pip5(2S5R)* (ring **A**) adopts the chair conformation placing C7 in the equatorial position thus avoiding unfavorable 1,3 diaxial interactions (Figure 11 **A**). The second pipecolic acid monomer *pip5(2R5S)* (ring **C**) is also predicted to adopt a chair conformation that places C11 in the equatorial position avoiding 1,3 diaxial interactions (Figure 11 **B**). The *pro4(2S4S)* (ring **E**) monomer is predicted to adopt an envelope conformation avoiding pseudo-1,3 diaxial interactions by placing C22 in the pseudo-equatorial position (Figure 12). The DKP ring linkages ring **B** and ring **D** are predicted to adopt shallow boat conformations placing their exo-cyclic substituents C17 and C28 respectively in the pseudo-equatorial positions.

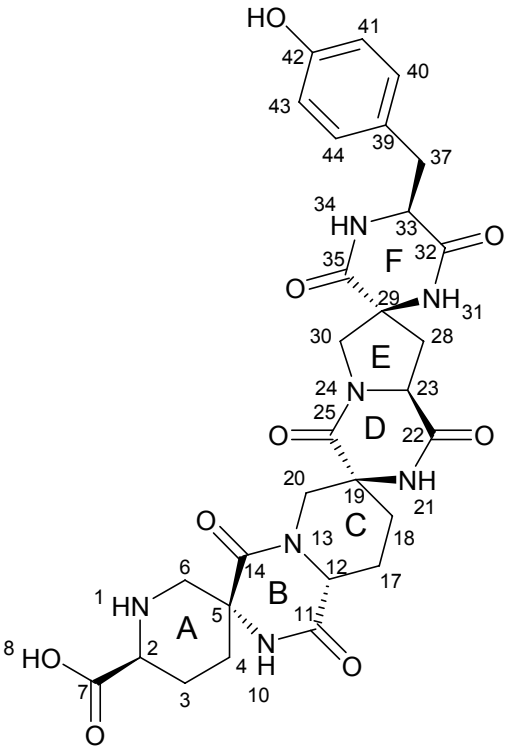

Figure 10: Atom numbering and ring nomenclature of 3.1.

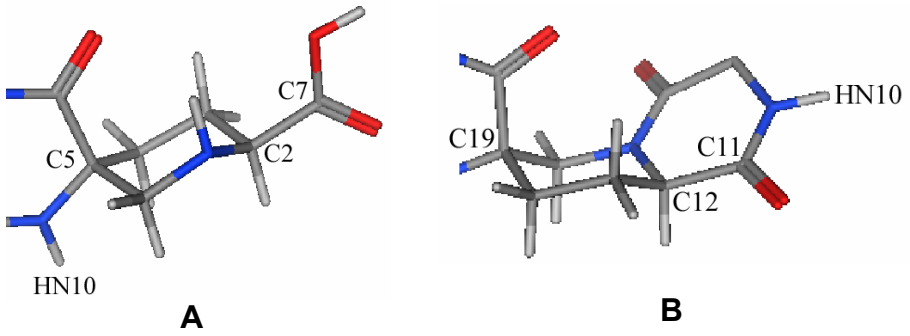

Figure 11: Lowest energy predicted conformations for *pip5(2S5R)* (A) and *pip5(2R5S)* (B) residues within the context of the full oligomer structure.

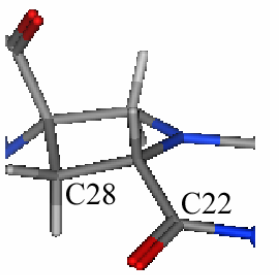

Figure 12: Lowest energy predicted conformation for *pro4(2S4S)* residue within the context of the full oligomer structure.

3.3 RESULTS

3.3.1 ^{13}C, ^{1}H Chemical Shift Assignment

In-depth structural analysis of **3.1** was performed by 2D-NMR in order to verify the connectivity, to confirm the assigned stereochemical assignments, and to help determine the conformation of the molecule in solution. The full structural assignment of ^{1}H and ^{13}C resonances of the hetero-oligomer were completed by performing ^{1}H, HMBC, and TOCSY NMR experiments on a 5 mM solution of **3.1** and HSQC-F1 dimension no decoupling and a ROESY NMR experiment on a 11 mM solution of **3.1** in 90% H_2O/D_2O with 20 mM acetate buffer at pH 3.4. This pH of 3.4 was used to slow the amide proton exchange as fast amide proton exchange with presaturation for solvent suppression will reduce signal intensity. The assignment of oligomer **3.1** was carried out using the software package SPARKY.

3.3.2 Conformation Determination Using ROESY Cross-Peaks

The ROESY spectrum provides cross peaks between protons that approach each other within 4Å. This close contact information was able to relate the amide hydrogens (HN10, HN21, HN31) with the methylene protons of the attached ring system allowing their diastereotopic assignment. In addition, ROESY cross-peaks observed for the three axial protons syn to each other on the two pipecolic acid rings **A** and **C** helped to confirm the chair conformation predicted by the Amer94 forcefield.[37] The relative intensities of the ROESY cross-peaks between protons were assigned as strong, medium, and weak based upon the Gaussian integrated intensities and are shown in Figure 13 as colored lines that suggest degrees of close-contact between the protons.

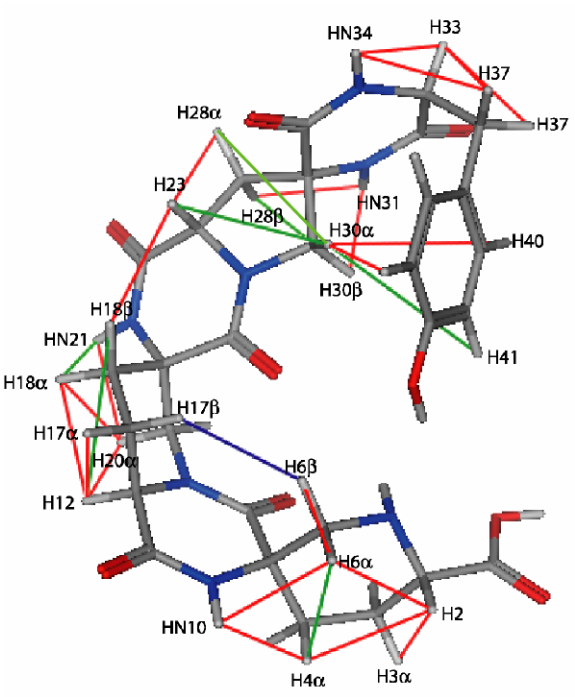

Figure 13: The lowest energy conformation of 3.1 shown with observed ROESY correlations. Correlated protons are connected by lines (strong – red, medium – green, weak – blue).

On ring **A,** cross-peaks are observed between protons H2-H3α, H2-H4α, and H2-H6α. In addition, cross-peak correlations are observed between H4α and H6α and between HN10-H6α and HN10-H4α. This information helps confirm the stereochemical assignment of ring **A** as well as support the predicted chair conformation with N10 in the equatorial position of ring **A**. On ring **C**, cross-peaks are seen between all pairs of protons H12, H17α, H18α, and H20α suggesting that they are on the same side of ring **C**. Protons HN21, H18α and H20α also show cross-peak correlations consistent with the designed stereochemistry. Once again, the observed correlations are in full agreement with the predicted chair conformation with N21 in the equatorial position of ring **C**. On ring **E**, a medium cross-peak is observed between protons H30α and H28α and a medium cross peak between H23 and H30α suggesting that these protons are on the same side of the ring. In addition, correlations can be seen between protons HN31-H28β and HN31-H30β which is consistent with the designed stereochemistry

ROESY cross-peaks were also observed between hydrogens on adjacent monomers which are consistent with the designed sequence of bis-peptide oligomer **3.1**. A strong cross-peak is observed between H23 and H18β, and a weak cross peak is observed between H6β and H17β. These particular close-contact correlations help to confirm that the DKP rings **B** and **D** occupy shallow boat conformations placing C17 and C6 into pseudo-axial positions and H23 and C18 into pseudo-axial positions. Lastly, ROESY cross-peaks between the protons on the aromatic side chain of the tyrosine and H30α suggests that the tyrosine folds back upon the oligomer as seen in previous studies.[19,22] The solution structure determined by NMR is in agreement with the predicted lowest energy conformation of **3.1** from MOE.[28]

Close contact information provided by ROESY cross-peak correlations provide insight into the molecular conformation of our bis-peptide oligomer. However, this alone cannot 100%

confirm the exact molecular conformation of **3.1** because ROESY correlations represent the average conformation of **3.1** if conformational switching is faster than the NMR timescale. Therefore, I turned to ^{1}H-^{1}H *J* couplings and residual dipolar coupling to obtain more NMR restraints on structure **3.1**.

3.3.3 Using ^{1}H-^{1}H couplings to Restrain Ring Conformations

^{1}H-^{1}H *J* couplings provide important dihedral information that can be of great value in structural determination by NMR[42]. Compared to the process of measuring *J*-couplings from 1D ^{1}H spectra, measuring *J*-couplings from 2D spectra is difficult. Delaglio and co-workers have developed an effective method to obtain *J*-coupling information from cross peaks in phase-sensitive COSY spectra by amplitude-constrained multiplet evaluation (ACME).[42] As the acronym suggests, this method operates by constraining the multiplet intensities assuming full relaxation of spin systems. Constraining the multiplet intensity for every set of cross-peaks eliminates several problems of multiplet extraction. For example, the large linewidth of 2D spectra results in a larger antiphase separation of lower intensity for the cross peaks leading to measured splittings larger than the true value (Figure 14).[42]

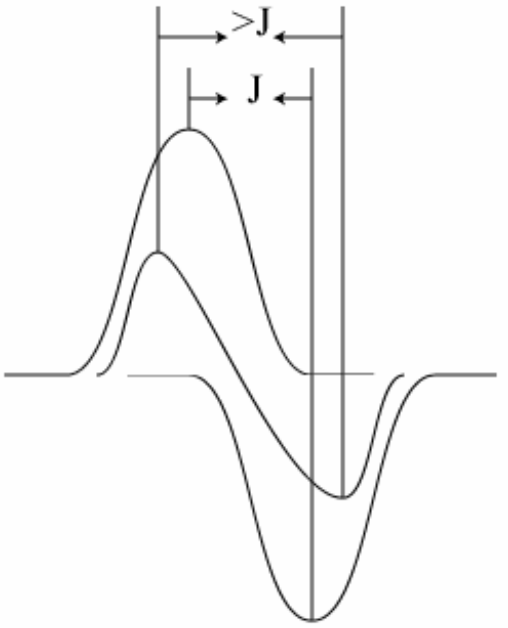

Figure 14: Effects of large linewidths in 2D COSYs that results in measuring larger J-couplings. The inner curve is the sum of the two antiphase peaks.

The amplitude value used to constrain all cross-peaks is determined by phasing the diagonal of the COSY spectrum to be absorptive, and then the intrinsic signal intensity is determined as the average intensity from the well resolved diagonal peaks. The diagonal is then removed from the phased COSY spectrum, and the *J*-couplings are calculated for each multiplet cross peak by a fitting process. The fitting process is completed by an iterative process of shifting and adding antiphase peaks constrained with the intrinsic signal intensity until the theoretical cross-peaks matches the original multiplet. The *J*-coupling constant is then measured from the antiphase peaks used to generate the model.

A phase-sensitive COSY with States acquisition mode (256 data points in F1 and 4K data points in the F2 dimension zero filed back to 4K for a resolution of 1.36 Hz/point) was acquired on a 7.0 mM solution of **3.1** in D_2O with 40 mM phosphate buffer at pH 7.5. Using ACME, the $^3J_{HH}$ coupling constants of each observed multiplet were determined (Table 1).

The dihedral angles of the COSY correlated protons in the lowest energy conformation of **3.1** (Figure 13) were measured in MOE[28]. The Karplus relation ($^3J_{HH} = 7 - \cos\theta + 5\cos 2\theta$) was then used to calculate theoretical $^3J_{HH}$ coupling constants from these measured dihedral angles. The experimentally measured *J*-couplings were consistent with predicted *J*-couplings (Table 1) providing evidence for the proposed energy minimized conformation of bis-peptide oligomer **3.1**. Unfortunately, the $^3J_{HH}$ coupling could not be measured for all COSY interactions on the *pip5(2S5R)* and *pip5(2R5S)* rings due to overlap of the *beta* and *gamma* protons. These cross-peaks resided too close to the diagonal peaks and were lost during the absorptive diagonal subtraction of the phased COSY spectrum.

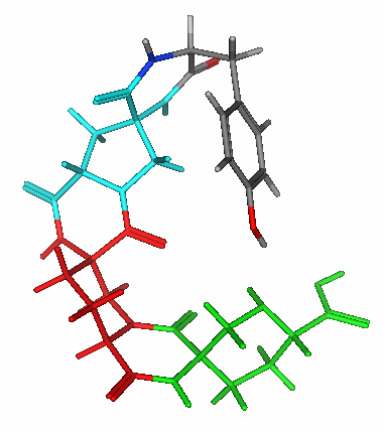

Resonance	$^3J_{HH}$ (measured)	Measured Dihedral Angle	$^3J_{HH}$ (calculated)
Ring **A**			
H3β – H2	12.0 Hz	171.6 °	12.8 Hz
H3α – H2	4.4 Hz	54.0 °	4.9 Hz
H3β – H4α	11.4 Hz	166.1 °	12.4 Hz
H3α – H4α	6.9 Hz	48.6 °	5.7 Hz
Ring **C**			
H17β – H12	12.1 Hz	178.0 °	13.0 Hz
H17α – H12	3.4 Hz	59.3 °	4.1 Hz
Ring **E**			
H28β - H23	10.7 Hz	161.4 °	11.9 Hz
H28α – H23	7.1 Hz	39.9 °	7.1 Hz

Table 1: Measured $^3J_{HH}$ coupling constants with ACME and calculated $^3J_{HH}$ values from lowest energy conformer of 3.1.

The *pip5(2S5R)* residue (ring **A**) is not constrained by a DKP linkage on the resin bound terminus. Thus ring **A** may be more conformationally mobile than the other rings in the bis-peptide oligomer. While ring **A** may be mobile, I set out to test the possibility of ring **A** possessing a well defined conformation. In order to test this hypothesis, ring **A** of the oligomer was flipped into three other possible conformations designated Twist Boat 1, Chair 2, and Twist Boat 2. These conformations were energy minimized with an Amber94 forcefield.[37] The dihedral angle of each set of COSY correlated protons on ring **A** was measured in MOE[28] for

each new ring **A** conformation. The $^3J_{HH}$ values were calculated ($^3J_{HH} = 7 - \cos\theta + 5\cos 2\theta$) for each conformation and compared to the ACME measured $^3J_{HH}$ coupling values (Table 2).

Resonance	Measured $^3J_{HH}$	Calculated $^3J_{HH}$		
		Twist Boat 1	**Chair 2**	**Twist Boat 2**
H3β – H2	12.0 Hz	11.2 Hz	2.8 Hz	8.5 Hz
H3α – H2	4.4 Hz	7.6 Hz	6.2 Hz	2.0 Hz
H3β – H4α	11.4 Hz	13.0 Hz	4.2 Hz	4.8 Hz
H3α – H4α	6.9 Hz	4.1 Hz	4.4 Hz	3.9 Hz

Table 2: Measured $^3J_{HH}$ and calculated $^3J_{HH}$ for allowable conformations of ring A.

It becomes evident that the only conformation of ring **A** that can coincide with the measured $^3J_{HH}$ coupling values is Twist Boat 1. In order to further verify if this conformation of ring **A** is a conformational possibility, the conformation of Twist Boat 1 was overlaid with the observed ROESY correlations that are shown in Figure 15 as colored lines that suggest degrees of close-contact between the protons. This new conformation of ring **A** does not support the strong ROESY correlations observed between H2 and H6α and between HN10 and H6α on ring **A**. In addition, the inter-residue weak correlation between H6β on ring **A** and H17β on ring **C** is not consistent with this twist boat conformation. This twist boat conformation of ring **A** would give rise to a ROESY cross-peak between H6α and H17β which I do not see in the 2D ROESY spectrum. Information from the ROESY cross-peaks and the $^3J_{HH}$ coupling constants support the idea that ring **A** is not in a static conformation but is rather flipping between an ensemble of allowed conformations. In order to help confirm this hypothesis, residual dipolar coupling was used to provide more insight into the conformational dynamics of bis-peptide oligomer **3.1**.

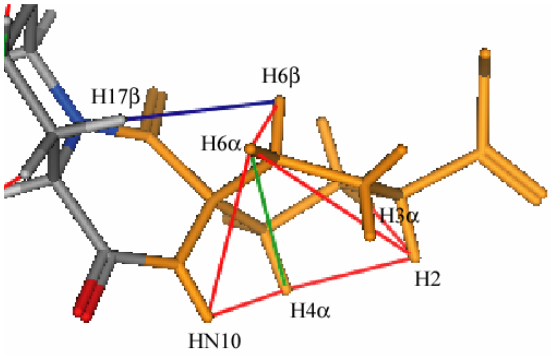

Figure 15: Twist Boat 1 conformation of ring A (orange) in 3.1 shown with observed ROESY correlations. Correlated protons are connected by lines (strong – red, medium – green, weak – green).

3.3.4 Residual Dipolar Couplings to Restrain Ring Conformations

Dipolar coupling is a through space interaction where the magnetic field of one nucleus, Q, effects the strength of the magnetic field of another nucleus, P. The amount of change in the magnetic field strength felt by nucleus P depends on the internuclear distance between P and Q (Figure 16).[43] This effect is dependent upon the magnetogyric ratios of the two nuclei (γ_P,γ_Q), the inverse cube of the distance between the nuclei (r_{PQ}^3), the magnitude of molecular alignment with the applied field B_0 (A_{ZZ}), and the angle of the internuclear vector with respect to B_0 (Figure 17).[43]

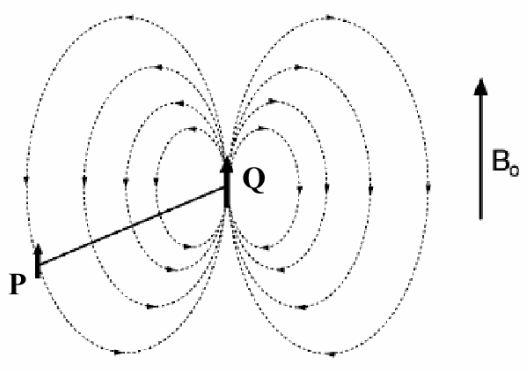

Figure 16 (adapted from ref [43]): Magnetic dipole-dipole coupling of Q and P.

$$D^{PQ}(\theta,\phi) = \frac{\hbar\gamma_P\gamma_Q}{4\pi^2 r_{PQ}{}^3} A_{ZZ}\left[\left(3\cos^2\theta - 1\right) + \frac{3}{2}R\sin^2\theta\cos\right.$$

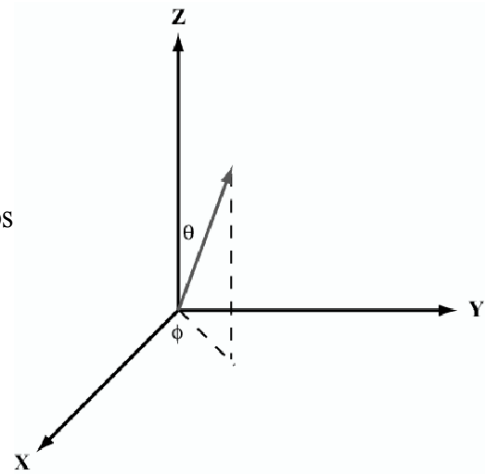

Figure 17[43]: (Eq 1) Describes the angular dependence of the internuclear vector on the magnitude of the dipolar coupling. (Fig 1) Shows the internuclear vector and its angle, θ, with the z axis, or B_0.

In solid state NMR, the dipolar couplings are very large interactions that give rise to very large splittings (on the order of 1000's of Hz). In contrast, when in solution the molecule rapidly rotates and the magnitude of the dipolar coupling averages exactly to zero. Residual dipolar coupling is an "in-between" case where the molecule is partially oriented with respect to B_o by a liquid crystal ordering medium.

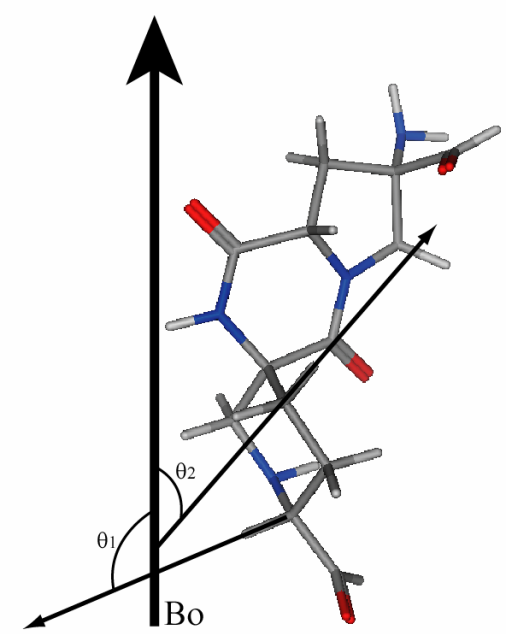

Figure 18: Representation of alignment tensor of solute molecule and a depiction of the internuclear vectors in orientation with applied magnetic field (B_0).

As briefly described above, RDCs contain information on the orientation of the internuclear vectors of the C-H bonds relative to the applied magnetic field. In particular, the molecule possesses a certain alignment tensor (Figure 18) with the ordering medium, a vector which describes the likelihood of the molecule aligning with a principal axis (x, y or z) and relates the molecule to Bo.[44] The alignment tensor represents one conformation of the solute molecule with respect to the applied magnetic field that is able to predict the experimentally measured RDCs. For rigid molecules with relatively defined molecular shape, such as our rigid bis-peptide oligomers, where all bond orientations are restrained by the inherent conformation preferences of our monomers we can deduce an alignment tensor that correctly describes the experimentally measured RDCs. Thus, residual dipolar couplings provide valuable restraints on internuclear vectors that can be used to relate the orientation of distant parts of the molecule relative to another allowing us to infer the global structure of the bis-peptide oligomer **3.1**.

By introducing weak alignment of our solute molecule in an applied magnetic field, I was able to measure RDCs acquired in a C-H coupled HSQC spectra. The alignment media chosen for the experiments was the filamentous bacteriophage, Pf1 phage[45], obtained from Asla Biotech. When subjected to an applied magnetic field, the phage particles align with the sides of the NMR tube. Steric and electrostatic interactions between the phage and the solute molecule give rise to the partial alignment of oligomer **3.1**.

Measuring the RDCs was accomplished by acquiring two C-H coupled HSQC spectra. The first was acquired (4k data points in the F1 dimension zero filed back to 4k and 4k data points in the F2 dimension) with no Pf1 phage present as to measure $^{1}J_{CH}$ coupling values with dipolar couplings averaging to zero, while the second was acquired (4k data points in the F1dimension zero filed back to 4k and 2k data points in the F2 dimension) with a 10 mg/mL concentration of phage to measure the $^{1}J_{CH} + {}^{1}D_{CH}$ coupling values.

These splittings can be measured in the higher resolution F2 dimension, but the alignment media causes significant line broadening leading to inaccuracy in locating the centers of the resonance peaks. Therefore when acquiring the HSQC spectra the 180 ° pulse on the ^{1}H channel during the t1 evolution period and decoupling during signal acquisition were eliminated. This causes the splitting values of the ^{1}H-^{13}C residual dipolar coupling to occur in the F1 dimension. Measuring the splittings in the F1 dimension reduces the line broadening problem allowing for better precision in measuring the $^{1}J_{CH}$ and $^{1}J_{CH} + {}^{1}D_{CH}$ values.

The measured $^{1}D_{CH}$ values are recorded in Table 3. When measuring the $^{1}J_{CH}$ and $^{1}J_{CH} + {}^{1}D_{CH}$ values for methylene units in the F1 dimension, it should be noted that the corresponding values represent the combined splitting ($^{1}J_{CH1} + {}^{1}J_{CH2} + {}^{1}D_{CH1} + {}^{1}D_{CH\,2}$) for the geminal pair. At first glance the RDCs seem very large on the order of 0 – 100 Hz (Table 3), but there was no

severe line broadening in the F1 dimension allowing for the precise determination of the middle of each resonance peak.

A Residual Dipolar Coupling Analysis Tool (REDCAT)[46] was used to evaluate the measured RDCs with respect to the energy minimized structure of bis-peptide oligomer **3.1**. The REDCAT program uses an input conformation and the measured RDC values to determine the best fit alignment tensor. I then used this alignment tensor to predict theoretical RDC values for the input structure and to determine the RMSD between the predicted and experimentally measured RDCs.

Resonance	$\sum^{1}D_{CH}$ (Hz)	Predicted $^{1}D_{CH}$ (Hz)
H2-C2	8.64	NA
H3α-C3 & H3β-C3	65.82	NA
H6α-C6 & H6β-C6	-40.04	NA
H12-C12	46.89	43.40
H17α-C17 & H17β-C17	65.82	68.68
H18α-C18 & H18β-C18	-5.66	-4.68
H20α-C20 & H20β-C20	64.07	70.07
H23-C23	-17.76	-17.68
H28α-C28 & H28β-C28	-113.15	-111.74
H30α-C30 & H30β-C30	-3.25	-3.04
H33-C33	-36.18	-36.84
2(H37-C37)	24.66	25.52

Table 3: Comparison of measured and calculated RDCs from best fit alignment tensor.

When the measured RDC values and the lowest energy conformer of **3.1** determined *in vacuo* using the Amber94[37] forcefield were entered into REDCAT, the algorithm did not find solutions when attempting to determine the best fit alignment tensor. However, when omitting the RDC values measured for the ^{1}H-^{13}C vectors on ring **A** and on the tyrosine residue, the REDCAT program was able to predict an RMSD value of 2.9 for the lowest energy conformer of

3.1 (Figure 19). As mentioned previously, it is possible for ring **A** to be conformationally mobile due to the lack of a second DKP linkage on the resin bound terminus. This suggests why the REDCAT algorithm breaks down when the RDCs from ring **A** are incorporated in the best alignment tensor fitting process. As a result these RDCs as well as the RDCs from the tyrosine residue were omitted during initial REDCAT analysis.

I found one conformation of rings **C**, **D**, and **E** that provide a good fit with the measured RDCs. In order to further reduce the RMSD fit for the backbone of ring **C**, ring **D**, and ring **E**, a dynamic search of ring **B** and ring **A** was conducted while fixing the rest of the molecule creating conformers with slightly varied H12–C12 vectors (Figure 19). This bond is part of the DKP linkage connecting ring **A** and ring **C** and its orientation will depend upon the conformation of ring **B** which is directly coupled to the conformation of ring **A**. The best fit structure **3.3** provided an RMSD of 2.4 (Figure 19).

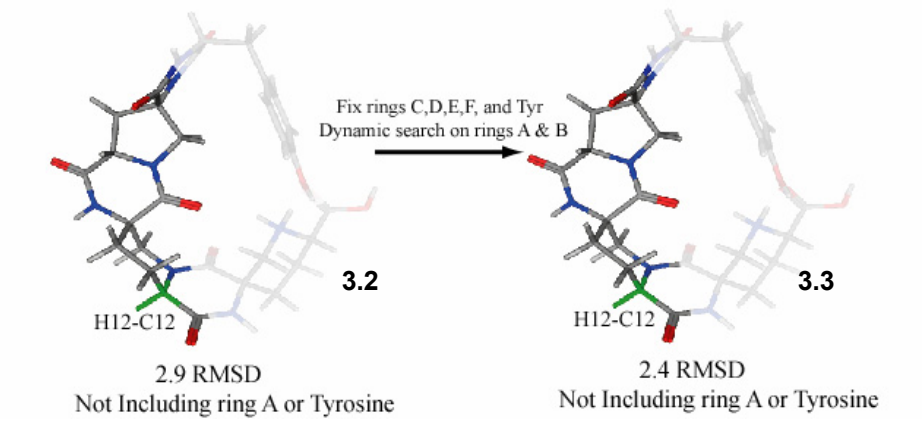

Figure 19: Rings C, D, E, F, and the tyrosine residue were held fixed in space while a molecular dynamic search was carried out on rings A and B. This refined the positioning of the H12-C12 vector leading to a lower RMSD value of 2.4.

To this point, the RDCs from the tyrosine residue have not been incorporated into the best alignment tensor RMSD fit. When including the H33-C33 RDC value with the best fit

structure **3.3** (Figure 19) in REDCAT[46], the RMSD value jumps to 11.4. In order to attain a better fit, a dynamic search of the tyrosine residue was carried out while holding the rest of the molecule rigid yielding best fit structure **3.4** with an RMSD of 2.2 (Figure 20). When including the combined H37-C37 RDC values with this new best fit structure **3.4**, the RMSD value jumps to 6.1. The H37-C37 bonds at the *beta* position of the tyrosine residue are free to rotate about the C33-C37 and C37-C39 bonds. In order to further reduce the RMSD best fit, both these C33-C37 and C37-C39 bonds were rotated at 5° increments. The RMSD value decreased to 2.2 with best fit structure **3.5** (Figure 20).

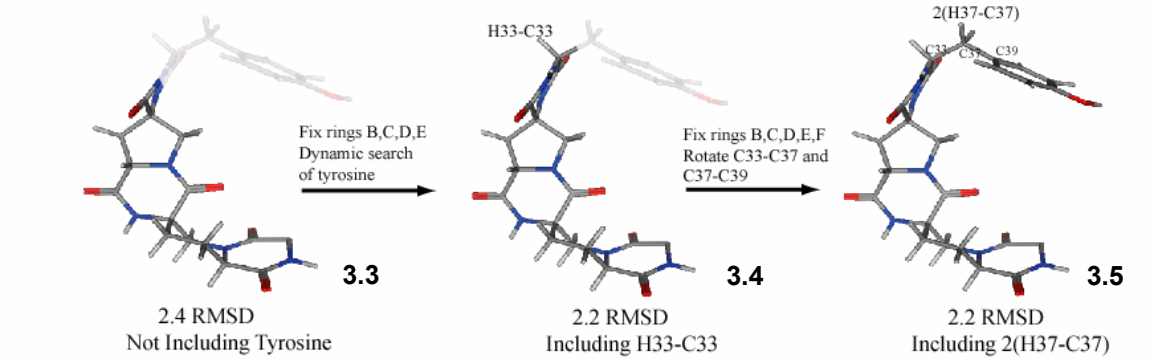

Figure 20: The refinement process of finding the tyrosine conformation with the best RMSD fit. First a dynamic search was done on the tyrosine residue followed by allowing C33-C37 and C37-C39 to search their conformational space.

The alignment tensor provided by the refined structure of **3.1** was used to predict theoretical RDCs (Table 3) for the inputted C-H bonds. It can be seen that these values are very consistent with the observed measured RDC values. A correlation plot between these predicted RDCs and experimentally measured RDCs is shown in Figure 21.

This refined structure of **3.1** treats the tyrosine residue as a static appendage, but it is possible for this terminal residue to rotate about the C33-C37 and C37-C39 bonds as well as there to be breathing motions of the DKP linkage (ring **F**) that connects this residue. The RMSD

best fit structure of 2.2 represents the tyrosine conformation that best represents the measured RDC values. However, close contact data from the 2D-ROESY spectrum is consistent with a conformation of the tyrosine residue that places it closer to H30α and H30β of ring **E**.

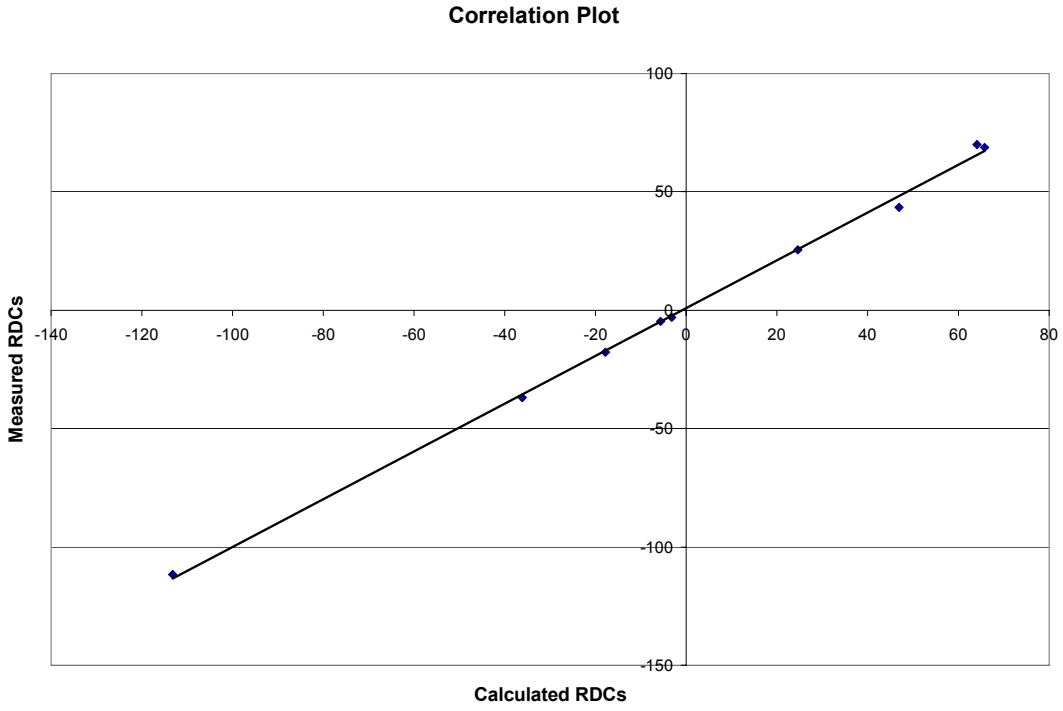

Figure 21: Correlation plot of experimentally measured RDCs vs. REDCAT[46] calculated RDCs.

In order to further demonstrate the utility of residual dipolar coupling in the structural determination and refinement of oligomer **3.1**, I systematically flipped the backbone rings of the scaffold into higher energy conformers. Ring **C** was flipped into its two boat conformations and the higher energy chair conformation, and ring **E** was flipped into its second envelope conformation. These new conformations of **3.1** were used to generate predicted RDCs with REDCAT that were compared to the experimental RDCs in the RMSD sense. It can be seen in

Table 4 that these other conformations do not fit well with the experimentally measured RDCs affording high RMSD values.

Conformation of 3.1	RMSD Value
3.5 (REDCAT refined conformation)	2.2
3.6 (Ring C Boat 1)	16.4
3.7 (Ring C Boat 2)	16.8
3.8 (Ring E Envelope 2)	17.5
3.9 (Ring C Chair 2)	23.0

Table 4: RMSD values acquired from the higher energy conformations of scaffold **3.1** during REDCAT analysis.

3.4 CONCLUSIONS

This final refined structure of bis-peptide oligomer **3.1** comprised of rings **C**, **D**, **E**, **F**, and the tyrosine residue has provided an RMSD value of 2.2 from REDCAT analysis and is in full agreement with the close contact information from the 2D-ROESY spectrum as well as the experimentally measured $^{3}J_{HH}$ coupling values. To conclude, I have confirmed that the backbone of **3.1** is structurally rigid and incapable of ring flipping. However, the beginning *pip5(2S5R)* residue, ring **A**, does not possess a DKP linkage on the resin bound terminus. There is no evidence by our analysis for a single conformation of ring **A**.

I have shown that there is a single conformation for rings **C**, **D**, **E**, **F**, and the tyrosine residue that is in agreement with ROESY cross-peak correlations, $^{3}J_{HH}$ coupling constants, and measured RDC values. This backbone does create a turn. In addition, I have shown that the amplitude constrained multiplet extraction[42] of $^{3}J_{HH}$ coupling constants provides important

dihedral angle information of our bis-peptide oligomers. Also, residual dipolar coupling has proven to be a great complimentary NMR technique to use for our bis-peptide structural determinations, and it is able to determine if a certain ring in our bis-peptide oligomers is conformationally mobile.

4.0 INITIAL DEVELOPMENT OF AN ACTUATED GLUCOSE SENSOR

4.1 INTRODUCTION AND BACKGROUND

Over the last decade, there has been an increasing interest in developing glucose sensors.[47-51] For the development of continuous *in vivo* glucose monitoring systems, implantable chemical glucose sensors[52-56] need to be in continuous contact with biological fluid in the human body so as to provide a constant measure of glucose levels in the body allowing the achievement of tight diabetes control. The idea of tight control is to maintain blood glucose levels as close to normal as possible so as to prevent or slow the progress of many complications that are characteristic of diabetes. These complications can include eye disease, kidney disease, and nerve disease.

Unfortunately, the use of glucose oxidase based sensors for glucose detection suffers problems of prolonged stability as well as the need for constant recalibration. Therefore, much effort has been devoted to synthesizing chemical glucose sensors.[48,49,51,57,58] In order to complete the task of creating an efficient chemical glucose sensor, a functional group that interacts with glucose needs to be identified as well as the appropriate construction of a three-dimensional scaffold structure.[49] Boronic acids are capable of binding diols at neutral pH (Figure 22) and have served the purpose of binding to saccharides very well, and have been used to create many examples diboronic acid sensors.[48,49,51,57-59]

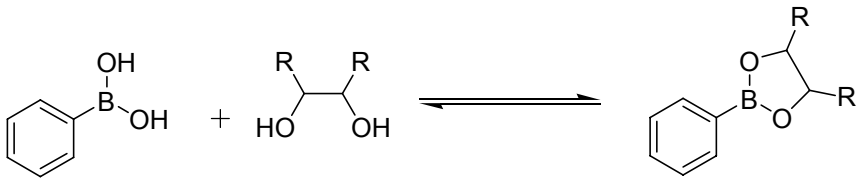

Figure 22: Binding between a phenylboronic acid and diol.

Typical glucose levels in the body range from 4 – 8 mM. Patients with diabetes attempt to maintain glucose levels within this range. Therefore, developing a glucose sensor that has a dissociation binding constant within this range would produce a sensor that is most responsive between the 1 -10 mM glucose range. Phenylboronic acids typically possess a K_d around 100 mM. Therefore, a designed chemical glucose sensor would need to show around a 20 fold increase in binding affinity for glucose in order to possess the sensitivity needed for detecting glucose levels in the 1 – 10 mM range.

Diboronic acid sensors have the ability to simultaneously bind to the 4,6 and 1,2 diol pairs on glucose. It has been investigated and determined that for the binding of glucose with these bis-boronic acid sensors there is a strong thermodynamic preference for the α-D-glucofuranose form[51] over the α-D-glucopyranose form (Figure 23). Upon binding to a boronic acid the pyranose form undergoes mutarotation to the furanose form relatively quickly in aqueous conditions.

α-D-glucopyranose boronic acid complex α-D-glucofuranose boronic acid complex

Figure 23: Boronic acid complexes of α-D-glucopyranose and α-D-glucofuranose respectively.

Of the vast array of small molecule based glucose sensors, most appear to be only water soluble after the addition of the sugar to the sensor itself. A powerful aspect of our synthetic approach is that we can independently adjust the water solubility of our glucose sensor without altering the other properties of the sensor. I have been focusing on creating an actuated water soluble-diboronic acid glucose sensor comprised of a rod-hinge-rod structure that converts from its disordered "open" form to an ordered "closed" form upon reversible binding to glucose (Figure 24). By placing "payloads" on each end of the hinged molecule, I can monitor the actuation (transition between the "open" and "closed" states) upon the addition of glucose so as to measure binding isotherms.

The "payloads" that can be used for our purposes can consist of a number of possibilities which includes a pair of fluorophores for fluorescence resonance energy transfer (FRET), excimers such as pyrene moieties, or even the possibility of anchoring one end of the glucose actuator to a single wall carbon nanotube with a charge on the other end so as to control the flow of current through the nanotube.

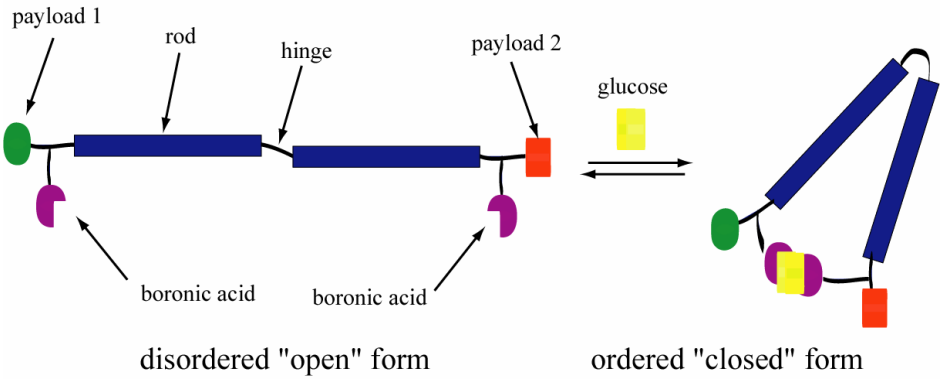

Figure 24: A schematic diagram of the molecular actuator glucose binding event.

There are many possibilities for the construction of this glucose sensor that is comprised of the rod-hinge-rod motif. For example, by controlling the overall structure and number of rotatable bonds within the hinge or by decreasing or increasing the number of bis-amino acid monomers in the rods I may be able to tune the degree of binding of the molecular actuator with glucose. In addition, changing the bis-amino acid monomers to different stereoisomers may also lead to changes in the glucose binding affinity. The studies provided to date demonstrate the initial development of this technology, and it must be stressed that many variants of the rod-hinge-rod system that consist of these variable hinge lengths, rod lengths, and monomer stereoisomers will be synthesized and studied.

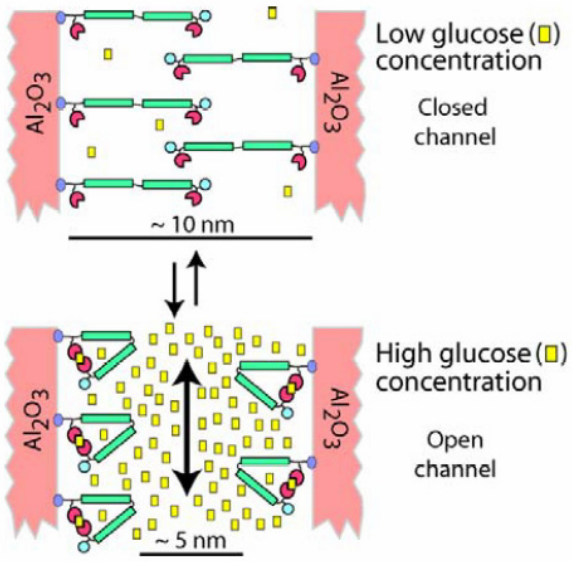

Figure 25: Molecular valves formed by attaching glucose sensitive molecular actuators to the insides of ~ 10 nanometer diameter alumina channels. At low glucose (yellow) concentrations the actuators will be disordered and block the channel ("valveclosed" state). In the presence of high glucose concentrations, the actuators will fold back, creating a channel with a diameter of about 5 nanometers, large enough to allow small proteins such as insulin to pass through ("valve-open" state).

It is an eventual goal of this project to someday create a working nanochannel based valve (Figure 25) by incorporating these actuating glucose sensors into alumina nanopore membranes. The opening and closing of these valves achieved by molecular actuation via reversible glucose binding will be able to control the flow of insulin and is dependent upon the overall glucose concentration present.

4.2 GLUCOSE SENSOR DESIGN AND SYNTHESIS

The first hinged molecule designed for these studies is composed of a rod-hinge-rod motif constructed from our bis-amino acids with an ornithine as the hinge (Figure 26). The rod segments of the molecule are each comprised of 4 *pro4(2R4R)* monomers that are connected by an ornithine hinge. The choice of "payloads" selected to actively monitor the glucose binding event are the naphthyl and dansyl fluorophore pair for monitoring with FRET. FRET is an energy transfer phenomenon that has been used extensively to measure distances and monitor structural changes in proteins and peptide sequences.[60-63]

One end of the actuator contains the dansyl fluorophore and one boronic acid as the other end has the naphthyl fluorophore and the second boronic acid. I set to determine the distance between the two fluorophores when in the disordered "open" state (~20-50 Å) and the distance between the fluorophore pairs when in the ordered "closed" state (~15-25 Å). I chose the naphthyl/dansyl pair because its Förster distance is ~22 Å which is the separation distance between the two fluorophores that yields 50% FRET efficiency. The FRET phenomenon works by exciting the naphthyl group which then emits energy by dipole-dipole resonance to the dansyl group that then emits energy at a longer wavelength of 520 nm. Upon titration of glucose, the

molecular actuator will bind to glucose in a 1:1 complex bringing the two fluorophores within a shorter distance. As the glucose concentration increases, all actuator molecules in solution bind to glucose. By measuring the efficiency of the fluorescence resonance energy transfer, I will generate binding isotherms that eventually will saturate at high glucose concentrations allowing the determination of binding constants.

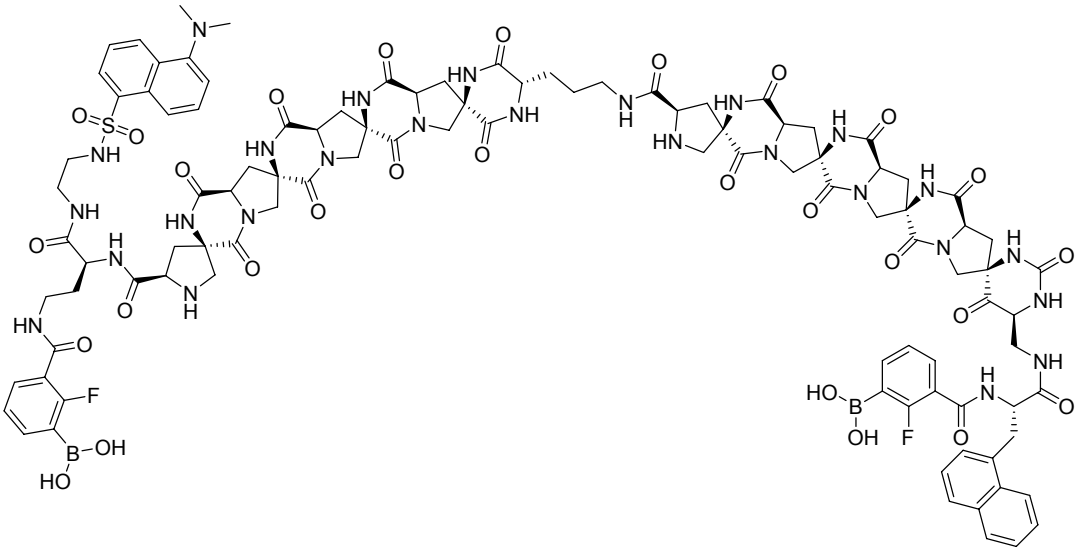

Figure 26: The molecular actuator structure of the diboronic acid glucose sensor.

Molecular modeling suggests that the glucose bound-closed actuator molecule positions the two fluorophores between 15-25 A° apart, and the unbound-open form places the fluorophores anywhere between 20-50 A° apart. I am hopeful for a large enough distance change that can be observed when monitoring the binding process between the actuated glucose sensor and glucose.

Choosing a boronic acid that will bind strongly at neutral pH is dependent upon the pKa of the boronic acid. In most but not all circumstances, the optimal pH at which the boronic acid will bind to diols is above the pKa of the boronic acid.[64] Therefore, introducing electron

withdrawing groups on the aryl ring in the ortho- or para- positions should stabilize the boronate form lowering the pKa of phenylboronic acid (pKa=8.8).[64,65] The phenyl boronic acid chosen for this study is 3-carboxy-2-fluorophenylboronic acid.

In addition, boronic acids are susceptible to boroxine formation (Figure 27) in organic solvents rendering them hard to work with.[66] To counteract this potential problem, boronic acids are protected with diols such as pinacol or neopentyl glycol. Hoeg-Jensen has developed solid-phase deprotection conditions for the pinacol boronate with N-methyldiethanolamine and 2M HCl[67], and hence this strategy was employed in my synthetic scheme.

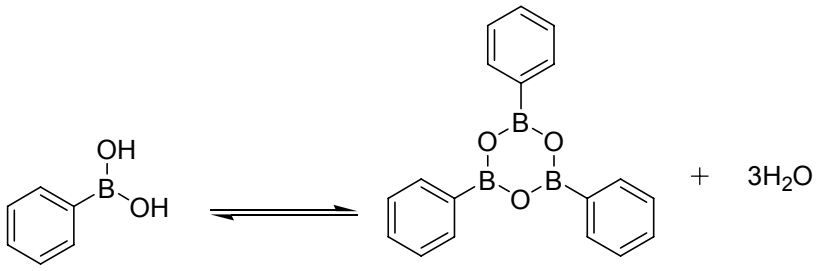

Figure 27: Formation of boroxine with boronic acids.

The 3-carboxy-2-fluorophenylboronic acid was protected as the pinacol boronate by treating it with pinacol in a mixture of 1:1 toluene/THF and evaporating to dryness under reduced pressure (Scheme 8) to yield **4.1**. The pinacol protecting group can then be subsequently cleaved via the two step treatment with 10% N-methyldiethanolamine/DMF and 10% 2M HCl/DMF.[67]

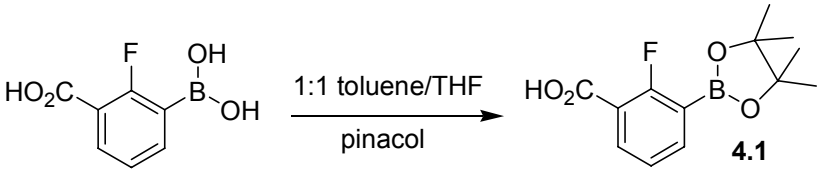

Scheme 8: Formation of pinacol boronate 4.1.

The scaffold was conveniently synthesized (Scheme 9) on the Dansyl NovaTag resin (Figure 28) installing the dansyl fluorophore on one end (C-terminus) of the molecular actuator. Upon cleavage of the linker with TFA, the C-terminus of the oligomer remains connected to the dansyl sulfonamide through a short linker (Figure 27).

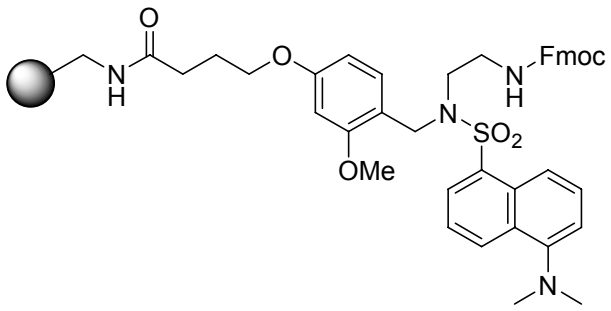

Figure 28: Dansyl NovaTag resin.

Scheme 9 shows the construction of the actuated glucose sensor, **4.3**. Initially a N-α-Fmoc-N-γ-1-(4,4-dimethyl-2,6-dioxocyclohex-1-ylidene)-3-methylbutyl-L-diaminobutanoic acid (Fmoc-Dab(ivDde)-OH) was coupled to resin followed by the sequential coupling of 4 Boc-*pro4(2R4R)* monomers. The flexible hinge was next installed as a N-α-Fmoc-N-δ-4-methyltrityl-L-ornithine (Fmoc-Orn(Mtt)-OH). The Fmoc protection in 20% piperidine/DMF was carried out for 2 hours to ensure a complete DKP closure between the ornithine and C-terminus connected Boc-*pro4(2R4R)* monomer. The side chain Mtt protecting group was subsequently removed with 1% TFA in DCM. To this free amine was coupled a Boc-*pro4(2R4R)* monomer followed by the sequential coupling of 3 additional Boc-*pro4(2R4R)* monomers. To the terminal Boc-*pro4(2R4R)* monomer was coupled a N-α-Fmoc-N-ε-4-methyltrityl-L-diaminoproprionic acid (Fmoc-Dpr(Mtt)-OH) followed by a 2 hours Fmoc deprotection in 20% piperidine/DMF to ensure a complete DKP closure between the Dpr(Mtt)

residue and C-terminus connected *pro4(2R4R)* monomer. The side chain Mtt protecting group was subsequently removed with 1% TFA in DCM and to this free amine was coupled an Fmoc-(S)-naphthylalanine installing the napthyl fluorophore on the end of the scaffold.

In order to simultaneously couple both 3-carboxy-2-fluorophenyl pinacol boronates to the oligomer, the ivDde side chain protecting group on the beginning Dab residue was removed with treatment to 1:4.5:4 hydrazine/All-OH/DMF yielding intermediate **4.2**. Next the pinacol boronate (**4.1**) of 3-carboxy-2-fluorophenylboronic acid was coupled to both free amines on the scaffold. The pinacol protecting groups of both boronic acids were then subsequently cleaved via the two step treatment with 10% N-methyldiethanolamine/DMF and 10% 2M HCl/DMF.[67]

The assembled scaffold was cleaved from the resin linker of the Dansyl NovaTag resin with 95% TFA, 2.5% H_2O, 2.5% TIPS to yield the globally Boc-deprotected scaffold. All diketopiperazines were closed in 20% piperidine in NMP and was completed after 1 day. The final closed product was precipitated in anhydrous ether and reverse phase purified by RP-HPLC on a 0-50 % gradient of MeCN/H_2O over 30 minutes to yield pure **4.3** (Figure 29).

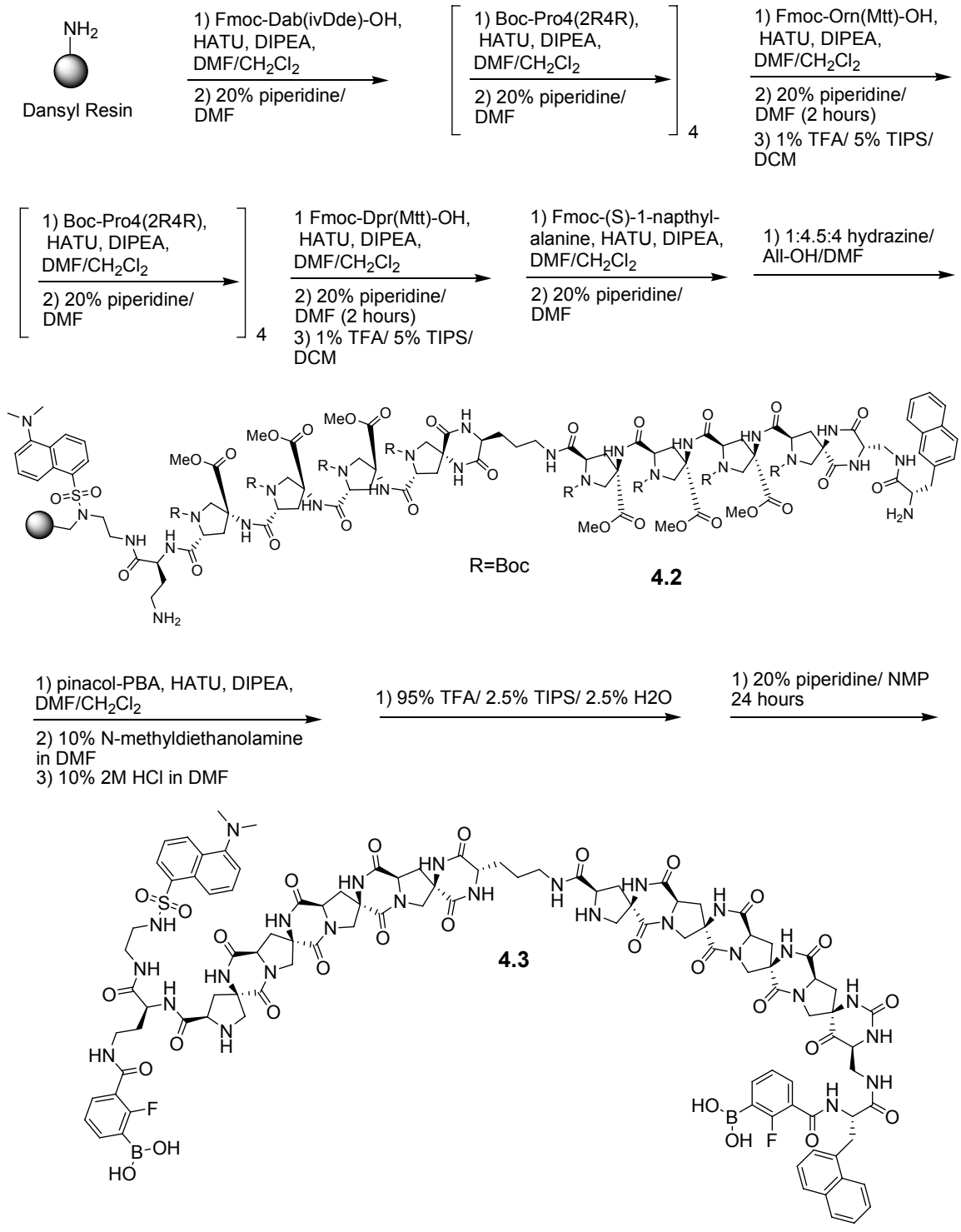

Scheme 9: Synthesis of the molecular actuator glucose sensor 4.3.

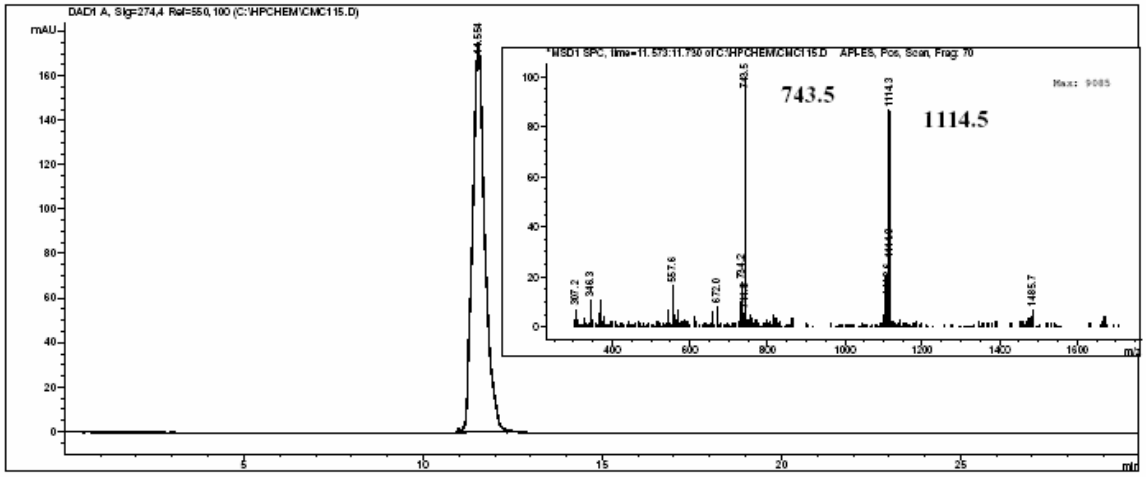

Figure 29: HPLC-MS: column, Waters XTerra MS C18 column; mobile phase , MeCN/water (0.1% formic acid), 5% to 95% MeCN over 30 minutes; flow rate, 0.4 mL/min; UV detection at 274 nm; tR 11.554 min; ES-MS m/z (ion) 1114.5 (M+2H+); m/z ion 743.5 (M+3H+).

4.3 TITRATING THE HINGED BIS-BORONIC ACID ACTUATOR WITH GLUCOSE

The molecularly actuated glucose sensor contains a donor napthyl group and an acceptor dansyl group separated on the two ends of the molecule. Glucose is known to bind dibornic acceptors via the 4,6 and 1,2 diol pairs, and thus the actuator should close upon binding to glucose in a 1:1 complex bringing the spatial orientation of the two fluorophores closer together inside the Förster distance of 22 Å. In order to observe this, excitation spectra were collected during the addition of D-glucose from 0-90 mM to a 10 μM solution of **4.3** in 0.1 M phosphate buffer at pH 7.4. The increase in fluorescence intensity can be observed in Figure 30 showing a relatively small increase in intensity changes. The K_d was approximated to be ~8 mM, a five fold increase from the monovalent K_d of 40 mM (Figure 31).

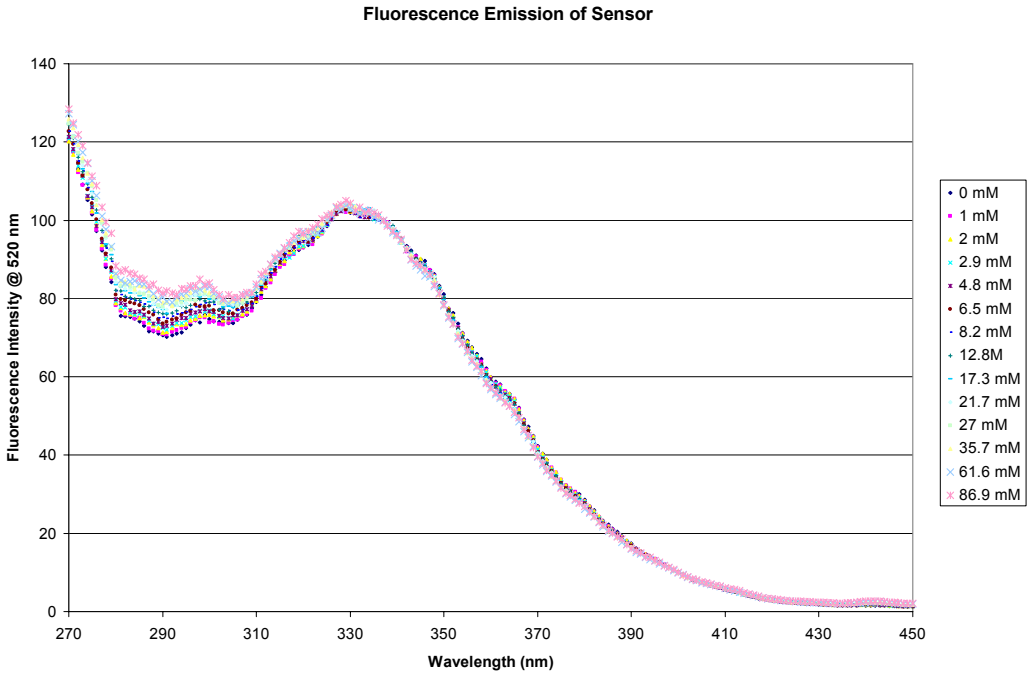

Figure 30: Excitation spectra of 4.3 (10 µM) upon addition of D-glucose (0-90 mM) at 25 °C in 0.1 M phosphate buffer at pH 7.4; λem = 520 nm. The spectra are normalized at 100 units at 337 nm.

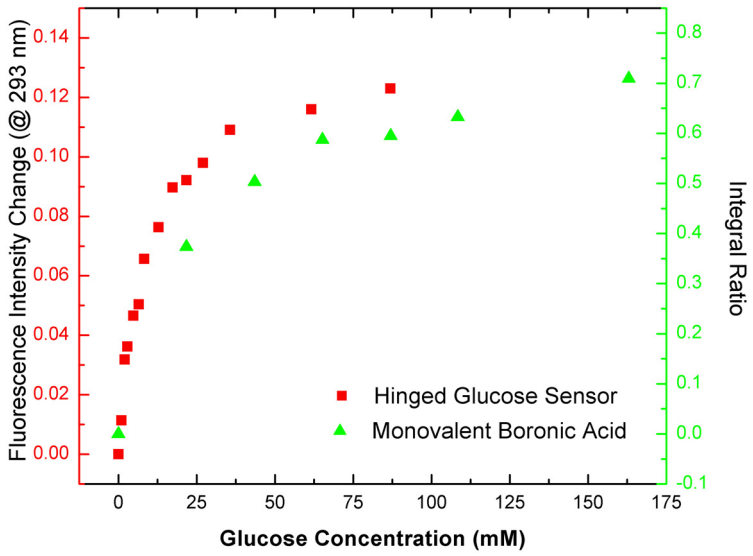

Figure 31: (RED) Fluorescence intensity changes as a function of glucose concentrations of 4.3 at 25 °C; 10 µM in 0.1 M phosphate buffer at pH 7.4; λex = 293 nm, λem = 520 nm. (Green) Integral ratio changes as a function of glucose concentration of monovalent boronic acid in 0.1 M phosphate at pH 7.4.

The fluorescence intensity changes are small (Figure 31) and can be rationalized when considering the number of possible conformations of the disordered "open" state of the glucose sensor. It is possible that instead of the rod-hinge-rod motif being more extended, that the disordered "open" form actuator holds the naphthyl and dansyl groups closer in proximity thus achieving a smaller change in separation upon converting to the ordered "closed" state when bound to glucose. As seen in Figure 32, there are many conformations available to the hinged molecule when the two rods are close to 90° to each other. The average distance between the two fluorophores was found to be 33 Å. This would apply a relatively small change in distance between the disordered and ordered states, and would account for the small increase in fluorescence intensity.

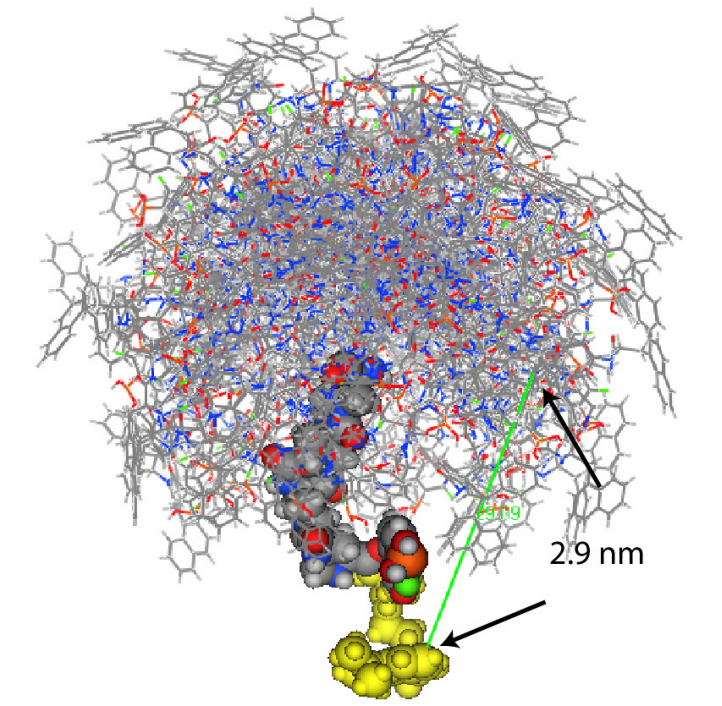

Figure 32: The overlaid structures of the available conformations of the disordered "open" hinged molecule 4.3. The average distance between the dansyl/naphthyl fluorophores is 33Å.

An ideal sensor would display a large change in fluorescence intensity when going from the unbound state to the bound state. In order to achieve this goal, the inherent design of the actuator can be altered by decreasing or increasing the length of the rods or by changing the flexibility of the hinge. Increasing the length of the rods would cause the fluorophores to have a larger distance separation when in the disordered unbound state possibly leading to larger distance changes between the bound and unbound states.

In addition to changing the structure of the sensor to achieve better sensitivity, I can also change the pair of fluorophores used for the FRET studies. The dansyl/naphthyl pair was synthetically convenient but a poor choice from the point of view of maximizing signal. Since it is easy to change the fluorophores, other signaling groups such as pyrenes for excimer formation will be explored as a potential signaling system. In addition to searching for different signaling groups, we will also explore different hinges with different molecular rod structures in order to improve signal. Currently the glucose actuated hinged molecule has a dissociation constant within the physiological range of glucose concentrations. I hope to create a few more hinged glucose sensors that are within the same physiological range.

This glucose molecular actuator opens the doorway for many important applications in the field of continuous glucose monitoring as well as in developing nanochannel based valves. Current studies are underway in attempting to create hinged sensors with increased signal between disordered “open” and ordered “closed” states. These studies will hopefully lead to improved glucose controlled molecular actuators.

5.0 EXPERIMENTAL SECTION

5.1 CHAPTER 2

General: CH_2Cl_2 was distilled from CaH_2 under N_2, and THF was distilled from Na/benzophenone under N_2. All other reagents were used as received from the company unless stated otherwise. All reactions were carried out in oven-dried glassware under an atmosphere of N_2 unless noted differently. Column chromatography was performed with ICN Silitech 32-63 D (60 A) grade silica gel using Redisep normal phase chromatography silica-gel columns on a Combiflash companion purification system from ISCO Inc. Analysis by TLC was carried out on EM Science Silica Gel 60 F_{254} plates with a 250 μm thickness. NMR experiments were performed on Bruker Advance 300 MHz, Bruker Advance DRX 500 MHz, or Bruker Advance DRX 600 Mhz spectrometers. All chemical shifts are reported relative to $CDCl_3$, DMSO-d_6, AcOD-d_4, or MeOD residual solvent peaks. When possible, rotational isomers were resolved by performing ^{1}H NMR experiments at 350 K in DMSO-d_6. IR spectra were obtained on a Nicolet Avatar E.S.P. 360 FT-IR. Optical rotations were obtained on a Perkin-Elmer 241 polarimeter. High resolution ESI-MS was performed on a Waters LC/Q-TOF instrument. HPLC-MS analysis was performed on a Hewlett-Packard Series 1050 instrument with a diode array detector, HP 1100 MS detector (ESI), using a Waters Xterra MS C_{18} column (3.5 μm packing, 4.6 X 100 mm). Purification by preparative HPLC was performed on a Varian Prostar 500 HPLC system with a Waters Xterra MS C_{18} column (5 μm packing, 30 X 100 mm) or a Waters Xterra MS C_{18}

column (5 μm packing, 10 x 100 mm). Analysis of 2D NMR data was performed using Sparky 3, T. D. Goddard and D.G. Kneller, University of California, San Francisco.

The following procedures parallel those in the synthesis of the pip5(2S5S) and the pro4(2S4S) (TFP ester version) bis-amino acid monomers[23, 25].

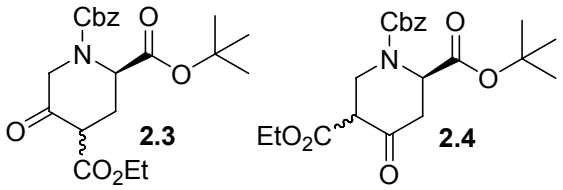

(*R*)-5-oxopiperidine-1,2,4-tricarboxylic acid 1-benzyl ester 2-*tert*-butyl ester 4-ethyl ester (2.3) and (*R*)-4-oxopiperidine-1,2,5-tricarboxylic acid 1-benzyl ester 2-tert-butyl ester 5-ethyl ester (2.4)

Compound **2.2**, **(*R*)-4-oxopyrrolidine-1,2-dicarboxylic acid 1-benzyl ester 2-*tert*-butyl ester,** (17.0 g, 53.3 mmol) was transferred to a 1000 ml round bottom flask containing a magnetic stir bar and fitted with a rubber septum. The flask was purged with nitrogen, and compound **2.2** was dissolved in anhydrous Et_2O (426 mL). The solution was cooled to 0 °C using an ice bath. The rubber septum was punctured with a 21G2 precision glide needle to allow venting for the remainder of the procedure. Boron trifluoride (13.5 mL, 106.7 mmol) was added dropwise via a continuous flow injector over a 30 minute period and then allowed to stir for 10 minutes. Ethyl diazoacetate (6.6 mL, 64.0 mmol) was added dropwise via a continuous flow injector over a 30

minute period. The solution was stirred for 2 hours at 0 °C and subsequently for 2 hours at room temperature. Saturated $NaHCO_3$ solution (250 mL) was slowly added to the solution and allowed to stir for 20 minutes. The resulting solution was transferred to a 2 L separatory funnel and was diluted with EtOAc (400 mL). The organic layer was separated and washed with saturated $NaHCO_3$ (3 x 250 mL) and then washed with brine (3 x 200 mL). The EtOAc layer was then dried over anhydrous $MgSO_4$, and filtered. The solution was concentrated by rotary evaporation and subsequently adsorbed onto celite. This was followed by purification with flash chromatography on a Combiflash companion purification system (140g silica column, 5-30% EtOAc/Hexanes gradient). Pure fractions were combined, and the solvent removed by rotary evaporation and under reduced pressure overnight. The resulting oil (12.8 g, 59% yield) was carried on directly to the next reaction.

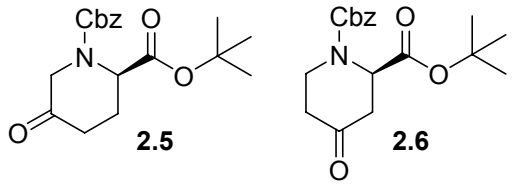

(*R*)-5-oxopiperidine-1,2-dicarboxylic acid 1-benzyl ester 2-*tert*-butyl ester (2.5) and (*R*)-4-oxopiperidine-1,2-dicarboxylic acid 1-benzyl ester 2-*tert*-butyl ester (2.6)

The mixture of **2.3** and **2.4** (25.1 g, 61.8 mmol) was dissolved in DMSO (185.3 mL) and transferred to a 500 mL round bottom flask containing a magnetic stir bar. H_2O (2.2 mL, 123.6 mmol) and NaCl (7.2 g, 123.6 mmol) were added. The flask was fitted with a reflux condenser and allowed to reflux at 150 °C for 4 hours. The solution was allowed to cool to room temperature and transferred to a 2 L separatory funnel and diluted with EtOAc (700 mL) and H_2O (150 mL). The EtOAc was separated, and the acqueous layer backwashed with EtOAc (2 x

200 mL). The EtOAc layers were combined and dried over anhydrous $MgSO_4$, and filtered. The solution was concentrated by rotary evaporation and subsequently adsorbed onto celite. This was followed with purification by flash chromatography on a Combiflash companion purification system (140g silica column, 5-30% EtOAc/Hexanes gradient, multiple columns were used). Fractions with the pure products (**2.5** or **2.6**) were combined separately, and the solvent was removed on the rotary evaporator and under reduced pressure overnight yielding **2.5** as an oil (6.0 g, 23.6% yield) and **2.6** as an oil (3.4 g, 13.6 % yield).

Characterization of **2.5**.

$[\alpha]^{23}_{D}$ = 5.8° (*c* 1.0, $CHCl_3$); IR (film) ν_{max} 2977, 1734, 1418, 1368, 1319, 1223, 1154, 1113, 1051, 963, 846, 746, 698; ^{1}H NMR (300 MHz, 77 °C, DMSO-*d*6) δ 7.50-7.54 (m, 5H), δ 5.24-5.33 (br s, 2H), δ 4.75 (t, 6 Hz, 1H), δ 4.37 (d, 18.3 Hz, 1H), δ 4.06 (d, 18.3 Hz, 1H), δ 2.59-2.70 (m, 1H), δ 2.47-2.55 (m, 1H), δ 2.40-2.43 (m, 1H), δ 2.24-2.30 (m, 1H), δ 1.56 (br s, 9H); ^{13}C NMR (75.4 MHz, 20 °C, DMSO-*d*6) δ 205.7, δ 171.1, δ 155.2, δ 136.8, δ 128.4, δ 81.8, δ 67.3, δ 54.8, δ 51.8, δ 35.7, δ 27.9, δ 23.2; HRMS-ES (*m/z*): 333.1592 ($C_{18}H_{23}NO_5$ + Na^+ requires 333.1576).

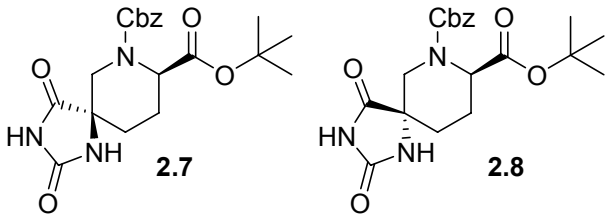

(5*R*,8*R*)-2,4Dioxo-1,3,7-triazaspiro[4.5]decane-7,8-dicarboxylic acid 7-benzyl ester 8-*tert*-butyl ester (2.7) and (5*R*,8*S*)-2,4Dioxo-1,3,7-triazaspiro[4.5]decane-7,8-dicarboxylic acid 7-benzyl ester 8-*tert*-butyl ester (2.8)

To a 350 mL pressure vessel containing a magnetic stir bar, ammonium carbonate (6.4 g, 66.6 mmol), potassium cyanide (1.5 g, 23.4 mmol), and deionized water (65 mL) were added. To this was added a solution of **2.5** (6.0 g, 18 mmol) in DMF (65 mL). The pressure vessel was sealed, and the reaction mixture stirred vigorously at 60 °C for 4 hours. The pressure vessel was cooled to 0 °C with an ice bath, and was opened cautiously. The solution was transferred to a 1000 mL Erlenmeyer flask and was acidified with 1 M HCl very slowly while stirring until no more bubbling occurred. The solution and precipitate were transferred to a 1000 mL separatory funnel and extracted with EtOAc (500 mL). The aqueous layer was extracted with EtOAc (3 x 200 mL). All organic layers were combined and washed with brine (3 x 200 mL), dried over anhydrous $MgSO_4$, and the solvent removed on the rotary evaporator and under reduced pressure overnight yielding a mixture of **2.7** and **2.8** in a ratio of 3:2 (determined by ^{1}H NMR in DMSO). This mixture is not separable by flash chromatography and is carried through directly to the next step.

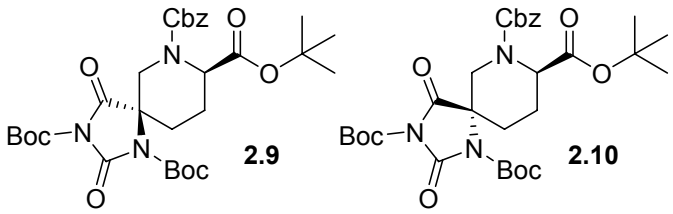

(5*R*,8*R*)-2,4-Dioxo-1,3,7-triazaspiro[4.5]decane-1,3,7,8-tetracarboxylic acid 7-benzyl ester 1,3,8-tri-*tert*-butyl ester (2.9) and (5*R*,8*S*)-2,4-Dioxo-1,3,7-triazaspiro[4.5]decane-1,3,7,8-tetracarboxylic acid 7-benzyl ester 1,3,8-tri-*tert*-butyl ester (2.10)

The crude mixture of **2.7** and **2.8** (7..3 g, 18.00 mmol, assuming 100% yield) was dissolved in dry THF (325 mL) and transferred to a 500 mL round bottom flask containing a magnetic stir bar. Di-*tert*-butyl dicarbonate (14.2 g, 65.22 mmol) and DMAP (.13 g, 1.1 mmol) were added. The reaction mixture was allowed to stir for 2 hours under N_2 flow. The solution was concentrated on a rotary evaporator and subsequently adsorbed onto celite. This was followed with immediate purification by flash chromatography on a Combiflash companion purification system (140g silica column, 5-30% EtOAc/Hexanes gradient). Fractions with pure products (**2.9** or **2.10**) were combined separately and concentrated on a rotary evaporator at room temperature. *In vacuo* drying yielded **2.9** as a white foamy solid (4.00 g, 36.8 % yield based on **2.5** over 2 steps) and **2.10** as a white foamy solid (1.64 g, 15.1 % yield based on **2.5** over 2 steps), as well as a mixture of **2.9** and **2.10** as a foamy solid (1.21g)

Less Polar **2.9**:

$[\alpha]^{23}_D$ = -5.0° (*c* 1.0, $CHCl_3$); IR (film) ν_{max} 2981, 1825, 1782, 1731, 1423, 1370, 1307, 1252, 1147, 976, 843, 756, 698; ^{1}H NMR ((300 MHz, 20 °C, DMSO-*d*6) δ 7.30-7.33 (m, 5H), δ 4.27-4.34 (m, 2H), δ 4.27 & 4.24 (rotamers, 1H), δ 3.91-4.12 (rotamers, 1H), δ 3.65 & 3.42 (rotamers,

1H), δ 2.10-2.17 (m, 2H), δ 2.01-2.07 (m, 2H), δ 1.49-1.52 (m, 27H); ^{13}C NMR (75.4 MHz, 20 °C, $CDCl_3$) δ 170.0, δ 169.8, δ 168.0, δ 167.9, δ 155.7, δ 155.6, δ 148.6, δ 148.5, δ 147.2, δ 147.1, δ 145.1, δ 136.5, δ 136.3, δ 128.6, δ 128.5, δ 128.2, δ 128.0, δ 127.8, δ 86.9, δ 85.5, δ 82.3, δ 67.9, δ 67.7, δ 60.6, δ 60.6, δ 54.1, δ 53.6, δ 43.1, δ 42.7, δ 28.0, δ, 27.8, δ 25.9, δ 22.4, δ 22.1; HRMS-ES (*m/z*): 626.2693 ($C_{30}H_{41}N_3O_{10}$ + Na^+ requires 626.2690).

More polar **2.10**.

$[\alpha]^{23}_D$ = 20.2° (*c* 1.0, $CHCl_3$); IR (film) ν_{max} 2980, 1827, 1786, 1740, 1456, 1423, 1369, 1318, 1254, 1142, 1089, 1057, 842, 754; ^{1}H NMR (300 MHz, 20 °C, DMSO-*d*6) δ 7.29-7.39 (m, 5H), δ 4.91-5.18 (m, 2H), δ 4.43 (t, 8.7 Hz, 1H), δ 4.22 (rotamers, 1H), δ 3.50 (rotamers 2d, 9.3 Hz, 1H), δ 2.04-2.26 (m, 3H) δ 1.87 (m, 1H) δ 1.29-1.51 (m, 27H); ^{13}C NMR (75.4 MHz, 20 °C, $CDCl_3$) δ 171.0, δ 170.6, δ 169.8, δ 169.5, δ 155.5, δ 155.4, δ 148.6, δ 148.5, δ 147.0, δ 145.0, δ 136.5, δ 136.3, δ 128.6, δ 128.5, δ 128.2, δ 128.0, δ 127.8, δ 87.1, δ 85.3, δ 81.8, δ 67.7, δ 67.4, δ 63.9, δ 63.8, δ 55.3, δ 55.0, δ 47.1, δ 46.8, δ 28.1, δ 28.0, δ 27.8, δ 27.7, δ 22.3, δ 21.6; HRMS-ES (*m/z*): 626.2676 ($C_{30}H_{41}N_3O_{10}$ + Na^+ requires 626.2690).

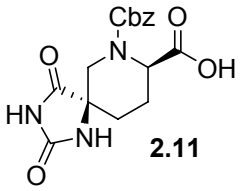

2.11

(5*R*,8*R*)-2,4-Dioxo-1,3,7-triazaspiro[4.5]decane-7,8-dicarboxylic acid 7-benzyl ester (2.11)

Compound **2.9** (52 mg, 0.086 mmol) was dissolved in a mixture of 3:7 TFA/DCM (~3.5 mL, 40 mL per mmol of **2.9**) and was transferred to a 25 mL round bottom flask fitted with a stir bar.

The mixture was stirred vigorously for 3 hours upon which it was diluted with toluene and concentrated by rotatory evaporation. This was repeated as to remove the TFA. *In vacuo* drying yielded a white foam **2.11**. This product was analyzed by NMR with no prior purification.

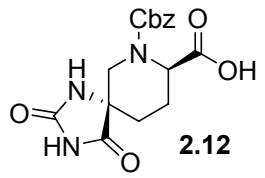

2.12

(5*R*,8*R*)-2,4-Dioxo-1,3,7-triazaspiro[4.5]decane-7,8-dicarboxylic acid 7-benzyl ester (2.12)

Compound **2.10** (42 mg, 0.069 mmol) was dissolved in a mixture of 3:7 TFA/DCM (~3.0 mL, 40 mL per mmol of **2.10**) and was transferred to a 25 mL round bottom flask fitted with a stir bar. The mixture was stirred vigorously for 3 hours upon which it was diluted with toluene and concentrated by rotatory evaporation. This was repeated as to remove the TFA. *In vacuo* drying yielded a white foam **2.12**. This product was analyzed by 2D-NMR with no prior purification.

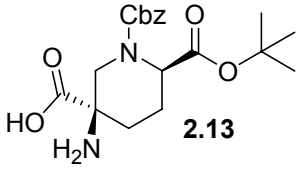

2.13

(2*R*,5*R*)-5-Aminopiperidine-1,2,5-tricarboxylic acid 1-benzyl ester 2-*tert*-butyl ester (2.13)

Compound **2.9** (8.8 g, 14.6 mmol) was dissolved in THF (58 mL) and transferred to a 250 mL round bottom flask. To this a 2M aqueous KOH solution (58 mL) was added. The reaction

mixture was stirred vigorously for 45 minutes at room temperature. The solution was transferred to a 500 mL separatory funnel and Et_2O (200 mL) was added. The aqueous layer was separated into a beaker and cooled to 0 °C with an ice bath. While under mechanical stirring, dropwise addition of 2M HCl resulted in a white precipitate. The pH was adjusted to 6.5 and monitored for 30 minutes. The solution was filtered through a medium frit sintered glass funnel, and the precipitate was washed with ice cold deionized water. The precipitate was allowed to air dry before *in vacuo* drying over anhydrous calcium sulphate followed by *in vacuo* drying in an oven at 40 °C yielding **2.13** as a white solid (5.27 g, 95.6 % yeld). $[\alpha]^{23}_D$ = 14.2° (*c* 1.0, MeOH); IR (film) ν_{max} 2975, 1735, 1690, 1616, 1498, 1432, 1403, 1352, 1222, 1153, 1109; ^{1}H NMR (300 MHz, 20°C, Ac-*d*3-OD) δ 7.24-7.31 (m, 5H), δ 5.01-5.15 (br m, 2H), δ 4.73 (br d, 1H), δ 4.35 (br t, 1H), δ 3.63 (d, 13.8 Hz), δ 2.38 (d, 14.1 Hz), δ 2.00-2.35 (m, 2H), δ 2.75 (m, 1H), δ 1.37 (m 9H); ^{13}C NMR (75.4 MHz, 20 °C, Ac-*d*3-OD) δ 177.8, δ 176.9, δ 156.3, δ 136.1, δ 128.4, δ 128.0, δ 127.8, δ 82.9, δ 68.1, δ ~58, δ ~55, δ ~45, δ 27.1, δ 22.1; HRMS-ES (*m/z*): 379.1887 ($C_{19}H_{27}N_2O_6$ + Na^+ requires 379.1869).

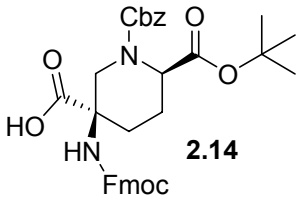

2.14

(*2R*,5*R*)-5-(9H-Fluoren-9-ylmethoxycarbonylamino)-piperidine-1,2,5-tricarboxylic acid 1-benzyl ester 2-*tert*-butyl ester (2.14)

To a 250 mL three neck round bottom flask containing a magnetic stir bar and fitted with a reflux condenser and rubber septa were added **2.13** (5.3 g, 13.9 mmol). This solid was suspended in

dry CH_2Cl_2 (70 mL). DIPEA (6.8 mL, 41.8 mmol) was added followed by the dropwise addition of chlorotrimethylsilane (3.7 mL, 29.3 mmol) with venting with a 21G2 precision glide needle. The resulting mixture was refluxed with nitrogen for 90 minutes. The solution was cooled to 0 °C with an ice bath, and 9-fluorenylmethyl chloroformate (4.0 g, 15.3 mmol) was added in one portion. The solution was warmed to room temperature overnight with stirring. The solution was concentrated by rotary evaporation, dissolved in EtOAc (150 mL), transferred to a 500 mL separatory funnel, and washed with 1 M HCl (3 x 75 mL). The aqueous layers were combined and backwashed with EtOAc (2 x 75 mL). The EtOAc layers were combined and washed with brine (3 x 75 mL) and then dried over anhydrous $MgSO_4$, and filtered. The solution was concentrated on a rotary evaporator and subsequently adsorbed onto celite. This was followed with immediate purification by flash chromatography on a Combiflash companion purification system (140g silica column, 0-10% MeOH/$CHCl_3$ gradient). Fractions with pure product were combined and solvent removed by rotary evaporation and under reduced pressure overnight to yield a white foamy solid **2.14** (5.8 g, 70 % yield). $[\alpha]^{23}_D$ = 9.4° (*c* 1.0, $CHCl_3$); IR (film) ν_{max} 3307, 3031, 2977, 2359, 2341, 1731, 1525, 1449, 1368, 1327, 1251, 1152, 1089, 1034, 1009, 757, 741, 697, 668; ^{1}H NMR (300 MHz, 77°C, DMSO-*d*6) δ 12.2 (br s, 1H), δ 7.86 (d, 7.5 Hz, 2H), δ 7.68 (d, 7.2, 2H), δ 7.52 (s, 1H), δ 7.28-7.44 (m, 9H), δ 5.10 (br s, 2H), δ 4.67 (d, 13.2 Hz, 1H), 4.58-4.64 (dd, 1H), δ 4.28-4.33 (m, 2H), δ 4.21 (dd, 1H), δ 2.95 (d, 13.2 Hz, 1H), δ 2.21 (m, 1H), δ 1.85-2.10 (m, 2H), δ 1.57 (ddd, 3 Hz, 12 Hz, 12 Hz, 1H), δ 1.4 (br s, 9H); ^{13}C NMR (75.4 MHz, 20 °C, $CDCl_3$) δ 175.2, δ 170.1, δ 156.0, δ 155.3, δ 143.6, δ 141.2, δ 141.1, δ 136.3, δ 128.3, δ 127.6, δ 127.0, δ 125.0, δ 119.8, δ 82.1, δ 67.6, δ 67.0, δ 56.6, δ 54.0, δ 46.9, δ 46.4, δ 28.9, δ 28.4, δ 27.9, δ 27.8, δ 27.4, δ 22.6; HRMS-ES (*m/z*): 601.2585 ($C_{34}H_{37}N_2O_8$ + Na^+ requires 601.2550).

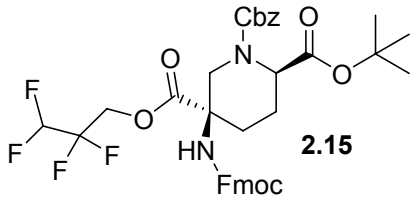

(2*R*,5*R*)-5-(9H-Fluoren-9-ylmethoxycarbonylamino)-piperidine-1,2,5-tricarboxylic acid 1-benzyl ester 5-(2,2,3,3 tetrafluoro) propyl ester 2-*tert*-butyl ester (2.15)

Compound **2.14** (5.4 g, 9.0 mmol) was dissoloved in dry CH_2Cl_2 (90 mL) and transferred to a 250 mL round bottom flask. To the solution were added DMAP (55 mg, .45 mmol, 0.05 equiv.) and 2,2,3,3-tetrafluoro propanol (1.6 mL, 18.1 mmol). The resulting solution was cooled with an ice bath and DCC (2.0 g, 9.5 mmol) was added in one portion. The reaction was complete after 5 hours of stirring and was monitored via TLC (5:1 $CHCl_3$/MeOH, visualized under UV). The solution was concentrated by rotary evaporation, the residue dissolved in 1:1 EtOAc/Hexanes (75 mL), and then filtered through a medium frit sintered glass funnel to remove byproduct DCU. The filtrate was concentrated by rotary evaporation and subsequently adsorbed on to celite. This was followed with immediate purification by flash chromatography on a Combiflash companion purification system (140g silica column, 0-50% EtOAc/Hexanes gradient). Pure fractions of **2.15** were combined, and the solvent removed by rotary evaporation and under reduced pressure overnight to yield a foamy white solid (4.8 g, 74% yield). $[\alpha]^{23}_D = 17.8°$ (*c* 1.0, $CHCl_3$); IR (film) ν_{max} 3323, 2978, 1761, 1728, 1526, 1450, 1426, 1368, 1321, 1255, 1117, 759, 741; ^{1}H NMR (300 MHz, 77°C, DMSO-*d*6) δ 7.91 (d, 7.5 Hz, 2H), δ 7.86 (s, 1H), 7.70 (d, 7.2 Hz, 2H), δ 7.30-7.50 (m, 9H), δ 6.42 (tt, 5.1 Hz, 47.1 Hz, 1H), δ 5.15 (br s, 2H), δ 4.66-4.76 (m, 2H), δ 4.47-4.61 (m, 2H), δ 4.40 (d, 2H), δ 4.25 (t, 8.7 Hz, 1H), δ 3.00 (d, br dd, 3.9 Hz, 10.5 Hz,

1H), δ 1.89 (m, 1H), δ 1.68 (dd, 3.6 Hz, 12.9 Hz, 1H), δ 1.45 (br s, 9H); ^{13}C NMR (75.4 MHz, 20 °C, $CDCl_3$) δ 170.1, δ 169.9, δ 155.6 & 155.5 (rotamers), δ 154.9, δ 143.6, δ 141.3, δ 136.2, δ 128.4, δ 128.0, δ 127.8, δ 127.7, δ 127.0, δ 124.8, δ 119.9, δ 113.9, δ 108.9, δ 82.2, δ 67.6, δ 66.9, δ ~61, δ 56.8, δ 53.7, δ 47.0, δ 46.7, δ 29.8, δ 27.9, δ 27.9, δ 27.5, δ 22.6; HRMS-ES (*m/z*): 737.2482 ($C_{37}H_{38}N_2O_8F_4$ + Na^+ requires 737.2462).

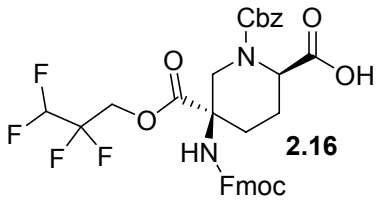

2.16

(2*R*,5*R*)-5-(9H-Fluoren-9-ylmethoxycarbonylamino)-piperidine-1,2,5-tricarboxylic acid 1-benzyl ester 5-(2,2,3,3 tetrafluoro) propyl ester (2.16)

Compound **2.15** (4.4 g, 6.2 mmol) was dissolved in dry CH_2Cl_2 (25 mL) and TFA (25 mL) and stirred vigorously for 2 hours in a 100 mL round bottom flask. The reaction was monitored via TLC (5:1 $CHCl_3$/MeOH, visualized under UV). The solution was concentrated by rotary evaporation and adsorbed onto celite. This was followed with immediate purification by flash chromatography on a Combiflash companion purification system (40g silica column, 0-10% MeOH/$CHCl_3$ gradient). Pure fractions of **2.16** were combined, and the solvent removed by rotary evaporation and under reduced pressure overnight to yield a foamy white solid (4.1 g, 100% yield). $[\alpha]^{23}_D$ = 11.2° (*c* 1.0, $CHCl_3$); IR (film) ν_{max} 3315, 3020, 2955, 1715, 1525, 1449, 1317, 1256, 1118, 1032, 966, 831, 758, 698, 667, 621; ^{1}H NMR (300 MHz, 77°C, DMSO-*d*6) δ 7.90 (d, 7.5 Hz, 2H), δ 7.82 (s, 1H), δ 7.70 (d, 7.2 Hz, 2H), δ 7.30-7.50 (m, 9H), δ 6.41 (tt, 5.1 Hz, 52.2 Hz, 1H), δ 5.16 (br s, 2H), δ 4.70-4.79 (m, 2H), δ 4.54-4.60 (m, 2H) δ 4.35-4.40 (d,

2H), δ (4.24, t, 6.6 Hz), δ 3.05 (br d, 13.5 Hz, 1H), δ 2.22 (br d, 13.5 Hz, 1H) δ 2.11 (br dd. 3.6 Hz, 10.5 Hzz, 1H), 1.89 (m, 1H), δ 1.67 (ddd, 3.6 Hz, 13.2 Hz, 13.2 Hz, 1H); ^{13}C NMR (75.4 MHz, 20 °C, $CDCl_3$) δ 175.1, δ 170.0, δ 155.9, δ 155.2, δ 143.4, δ 141.3, δ 135.8, δ 128.4, δ 128.1, δ 127.7, δ 127.0, δ 124.7, δ 120.0, δ 109.0, δ ~82, δ 68.0, δ 67.1, δ 60.0, δ 56.5, δ 53.1, δ 49.9, δ 46.9, δ 33.3, δ 29.8, δ 22.8 and 22.3 (rotamers); HRMS-ES (*m/z*): 681.1804 ($C_{33}H_{30}N_2O_8F_4$ + Na^+ requires 681.1836).

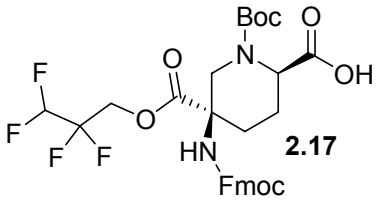

2.17

(2*R*,5*R*)-5-(9H-Fluoren-9-ylmethoxycarbonylamino)-piperidine-1,2,5-tricarboxylic acid 1-*tert*-butyl ester 5-(2,2,3,3 tetrafluoro) propyl ester (2.17)

Compound **2.16** (3.71 g, 5.73 mmol) was dissolved in dry THF (50 mL) and transferred to a 100 mL round bottom flask. To the solution were added 10 wt % Pd/C (371 mg, 10% by wt **2.16**) and di-*tert*-butyl dicarbonate (3.1 g, 14.1 mmol). The solution was degassed by vacuum filtration and backfilled with H_2 via a balloon (cycle repeated 3 times). The reaction progress was monitored via HPLC. The progress stalled and therefore DIPEA (2.82 mmol, 0.5 equiv) was added, and the conversion was completed after 7 hours. The solution was filtered through fluted filter paper, and the residual Pd/C washed repeatedly with $CHCl_3$. The solution was concentrated by rotary evaporation and adsorbed onto celite. This was followed by immediate purification by flash chromatography on a Combiflash companion purification system (40g silica comlumn, 0-10% MeOH/$CHCl_3$ gradient). All pure fractions were combined, and the solvent

removed by rotary evaporation and under reduced pressure overnight yielding a white foamy solid **2.17** (2.2 g, 63 % yield). $[\alpha]^{23}_D$ = 14.0° (*c* 1.0, $CHCl_3$); IR (film) ν_{max} 3306, 3015, 2979, 1715, 1958, 1477, 1450, 1417, 1394, 1369, 1320, 1255, 1158, 1119, 1030, 759, 741; ^{1}H NMR (300 MHz, 77°C, DMSO-*d*6) δ 7.90 (d, 7.5 Hz, 2H), δ 7.80 (s, 1H), δ 7.71 (d, 8.1 Hz, 2H), δ 7.32-7.50 (m, 4H), 6.43 (tt, 5.4 Hz, 52.2 Hz, 1H), δ 4.62 (br d, 12.9 Hz, 2H), δ 4.49-4.67 (m, 3H), δ 4.37 (d, 6.3 Hz, 2H), δ 4.25 (t, 6.6 Hz, 1H), δ 3.00 (d, 6.3 Hz, 1H), δ 2.26 (br d, 13.5 Hz, 1H), δ 2.06 (dd, 1H), δ 1.83-1.96 (m, 1H); ^{13}C NMR (75.4 MHz, 20 °C, DMSO-*d*6) δ 172.3, δ 170.3, δ 155.2, δ 154.1, δ 143.7, δ 140.7, δ 127.6, δ 127.0, δ 125.0, δ 120.1, δ 79.5, δ 79.1, δ 65.7, δ 59.8, δ 56.5 & 56.4 (rotamers), δ 53.5, δ 46.6, δ 45.8, δ 29.2, δ 28.2, δ 27.8, δ 27.4, δ 22.2; HRMS-ES (*m/z*): 647.1996 ($C_{30}H_{32}N_2O_8F_4$ + Na^+ requires 647.1992).

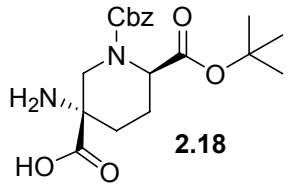

2.18

(2*R*,5*S*)-5-Aminopiperidine-1,2,5-tricarboxylic acid 1-benzyl ester 2-*tert*-butyl ester (2.18)

The general procedure for the synthesis of compound **2.13** was followed for the synthesis of **2.18** (1.0 g, 100% yield, salts were present) starting with compound **2.10** (1.7 g, 2.7 mmol). $[\alpha]^{23}_D$ = 16.4° (*c* 1.0, $CHCl_3$); IR (film) ν_{max} 2972, 1731, 1698, 1597, 1532, 1449, 1366, 1325, 1254, 1210, 1150, 1125; ^{1}H NMR (300 MHz, 20°C, Ac-*d*3-OD) δ 7.25-7.32 (m, 5H), δ 4.99-5.22 (m, 2H), δ 4.74-4.76 (rotamers) (m, 1H), δ 4.34 (d, 14.7 Hz, 1H), δ 3.43-3.60 (rotamers) (m, 1H), δ 1.98-2.20 (m, 4H), δ 1.34-1.37 (m, 9H); ^{13}C NMR (75.4 MHz, 20 °C, Ac-*d*3-OD) δ 174.0, δ 170.7 & 170.4 (rotamers), δ 158.0 & 157.9 (rotamers), δ 137.0, δ 129.4, δ 129.2, δ 129.0, δ

128.9, δ 83.6, δ 69.1, δ 60.4, δ 55.3 & 54.9 (rotamers), δ 46.6 & 46.3 (rotamers), δ 28.1, δ 28.0, δ 21.2; HRMS-ES (*m/z*): 379.1855 ($C_{19}H_{27}N_2O_6$ + Na^+ requires 375.1869).

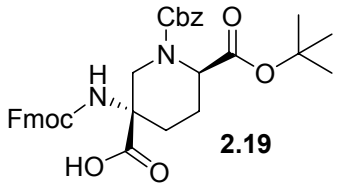

2.19

(2R,5S)-5-(9H-Fluoren-9-ylmethoxycarbonylamino)-piperidine-1,2,5-tricarboxylic acid 1-benzyl ester 2-*tert*-butyl ester (2.19)

The general procedure for the synthesis of compound **2.14** was followed for the synthesis of **2.19** (1.2 g, 71 % yield) starting with compound **2.18** (1.0 g, 2.7 mmol). $[\alpha]^{23}_D$ = 17.9° (*c* 1.0, $CHCl_3$); IR (film) ν_{max} 3325, 2977, 1731, 1524, 1449, 1368, 1322, 1285, 1249, 1156, 1132, 1071, 1003, 757, 740, 697; ^{1}H NMR (300 MHz, 77°C, DMSO-*d*6) δ 7.88 (d, 7.5 Hz, 2H), δ 7.69 (d, 6.9 Hz, 2H), δ 7.20-7.47 (m, 9H), δ 5.03 (br s, 2H), δ 4.65 (m, 2H), δ 4.2. (br s, 1H), δ 3.32, (br s, 2H), δ 1.93-2.30 (m, 3H), δ 1.63 (ddd, 5.1 Hz, 14.7 Hz, 14.7 Hz, 1H), δ 1.41 (br s, 9H); ^{13}C NMR (75.4 MHz, 20 °C, $CDCl_3$) δ 176.3 & 175.9 (rotamers), δ 169.5, δ 156.6 & 156.4 (rotamers), δ 155.7, δ 143.7 &143.5 (rotamers), δ 141.3, δ 135.9, δ 128.5, δ 128.2, δ 128.0, δ 127.7, δ 127.0, δ 125.0, δ 119.9, δ 82.4, δ 67.9 & 67.1 (rotamers), δ 57.9 & 57.3 (rotamers), δ 54.5 & 53.9 (rotamers), δ 47.0, δ 46.2, δ 28.0, δ 27.9, δ 27.5, δ 25.6, δ 21.4; HRMS-ES (*m/z*): 623.2383 ($C_{34}H_{36}N_2O_8$ + Na^+ requires 623.2369).

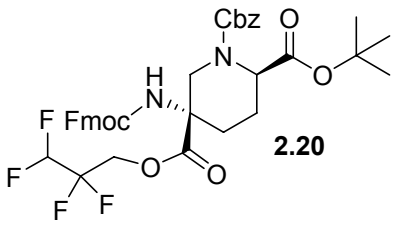

2.20

(2*R*,5*S*)-5-(9H-Fluoren-9-ylmethoxycarbonylamino)-piperidine-1,2,5-tricarboxylic acid 1-benzyl ester 5-(2,2,3,3 tetrafluoro) propyl ester 2-*tert*-butyl ester (2.20)

The general procedure for the synthesis of compound **2.15** was followed for the synthesis of **2.20** (1.1g, 87% yield) starting with compound **2.19** (1.1 g, 1.8 mmol). $[\alpha]^{23}_{D} = 18.8°$ (*c* 1.0, $CHCl_3$); IR (film) ν_{max} 3324, 3016, 2977, 2942, 1760, 1731, 1524, 1450, 1394, 1369, 1286, 1188, 1155, 1112, 1081, 1014, 966, 845, 829, 758, 742, 697; ^{1}H NMR (300 MHz, 77°C, DMSO-*d*6) δ 7.86 (d, 7.5 HZ, 2H), δ 7.76 (br s, 1H), δ 7.65 (d, 6.9 Hz, 2H), δ 7.21-7.46 (m, 9H), δ 6.41 (tt, 4.8 Hz, 52.2 Hz, 1H), δ 5.05 (br s, 2H), δ 4.72 (d, 1H), δ 4.48-4.64 (m, 3H), 4.15-4.29 (m, 3H), δ 3.31 (br s, 1H), δ 1.91-2.18 (m, 3H), δ 1.65 (m, 1H), δ 1.42 (br s, 9H); ^{13}C NMR (75.4 MHz, 20 °C, $CDCl_3$) δ 170.4, δ 169.4, δ 156.5 & δ 156.1, δ 155.1, δ 143.6, δ 141.3, δ 135.9, δ 128.5, δ 128.3, δ 128.0, δ 127.7, δ 127.0, δ 124.9, δ 120.0, δ 113.8, δ 82.5, δ 67.9, δ 67.0, δ 60.4, δ 58.0 & 57.5 (rotamers), δ 54.4 & 53.7 (rotamers), δ 47.3 & 47.1 (rotamers), δ 46.1, δ 28.3, δ 27.9, δ 27.8, δ 25.6, δ 21.3; HRMS-ES (*m/z*): 737.2422 ($C_{37}H_{38}N_2O_8F_4 + Na^+$ requires 737.2462).

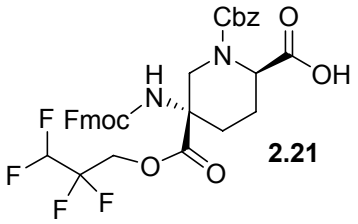

2.21

(2*R*,5*S*)-5-(9H-Fluoren-9-ylmethoxycarbonylamino)-piperidine-1,2,5-tricarboxylic acid 1-benzyl ester 5-(2,2,3,3 tetrafluoro) propyl ester (2.21)

The general procedure for the synthesis of compound **2.16** was followed for the synthesis of **2.21** (0.83g, 92% yield) starting with compound **2.20** (1.0 g, 1.4 mmol). $[\alpha]^{23}_{D}$ = 11.3° (*c* 1.0, $CHCl_3$); IR (film) ν_{max} 3323, 3032, 2952, 1717, 1517, 1449, 1284, 1112, 1013, 965, 859, 831, 741, 697, 667; ^{1}H NMR (300 MHz, 77°C, DMSO-*d*6) δ 7.86 (d, 7.5 Hz, 2H), δ 7.76 (br s, 1H), δ 7.65 (d, 7.2 Hz, 2H), δ 7.21-7.45 (m, 9H), δ 6.41 (tt, 4.8 Hz, 52.2 Hz, 1H), δ 5.05 (br s, 2H), δ 4.80 (br d, 4.8 Hz, 1H), δ 4.47-4.64 (m, 3H), δ 4.15-4.28 (m, 3H), δ 3.35 (br s, 1H), δ 1.93-2.19 (m, 3H), δ 1.69 (m, 1H); ^{13}C NMR (75.4 MHz, 20 °C, $CDCl_3$) δ 175.2 & 174.8, δ 170.3, δ 156.5, δ 155.4, δ 143.4, δ 141.3, δ 135.6, δ 128.5, δ 128.2, δ 127.9, δ 127.7, δ 127.0, δ 120.0, δ 113.8, δ 109.2, δ 105.8, δ 68.2, δ 67.0, δ 60.2, δ 57.9 & 57.2 (rotamers), δ 53.6 & 53.0 (rotamers), δ 47.0, δ 45.8, δ 27.6, δ 20.9; HRMS-ES (*m/z*): 681.1793 ($C_{33}H_{30}N_2O_8F_4$ + Na^+ requires 681.1836).

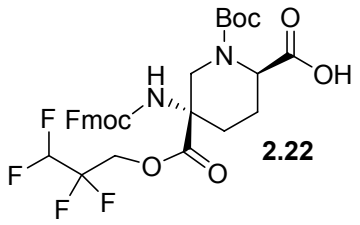

2.22

(2*R*,5*R*)-5-(9H-Fluoren-9-ylmethoxycarbonylamino)-piperidine-1,2,5-tricarboxylic acid 1-*tert*-butyl ester 5-(2,2,3,3 tetrafluoro) propyl ester (2.22)

The general procedure for the synthesis of compound **2.17** was followed for the synthesis of **2.22** (.32 g, 51 % yield) starting with compound **2.21** (.66 g, 1.0 mmol). $[\alpha]^{23}_{D}$ = 4.27° (*c* 0.5, $CHCl_3$); IR (film) ν_{max} 3323, 2976, 1757, 1716, 1521, 1450, 1477, 1394, 1368, 1267, 1185, 1154, 1113, 1014, 965, 851, 759, 666, 620; ^{1}H NMR (300 MHz, 77°C, DMSO-*d*6) δ 7.91 (d, 7.5 Hz, 2H), δ 7.72 (d, 7.5 Hz, 2H), δ 7.32-7.50 (m, 4H), δ 6.45 (tt, 5.1 Hz, 52.2 Hz, 1H), δ 4.50-4.80 (m, 4H), δ 4.21-4.49 (m, 3H), δ 3.55-3.78 (m, 1H), 1.94-2.14 (m 3H), δ 1.0-1.76 (m, 1H), δ 1.40 (br s, 9H); ^{13}C NMR (75.4 MHz, 20 °C, DMSO-*d*6) δ 172.5, δ 171.4, δ 155.3, δ 154.3, δ 143.3, δ 140.4, δ 127.8, δ 126.3, δ 125.7, δ 120.9, δ 118.8, δ 80.3, δ 78.8, δ ~67.0, δ ~59.5, δ 56.5, δ 5436, δ 52.3, δ 46.3, δ 45.4, δ 28.4, δ 26.7, δ ~21; HRMS-ES (*m/z*): 647.2.

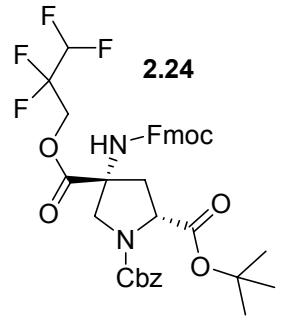

(2*R*,4*R*)-5-(9H-Fluoren-9-ylmethoxycarbonylamino)-proline-1,2,4-tricarboxylic acid 1-benzyl ester 4-(2,2,3,3 tetrafluoro) propyl ester 2-*tert*-butyl ester (2.24)

The general procedure for the synthesis of compound **2.15** was followed for the synthesis of **2.24** (1.7 g, 70% yield) starting with compound (2R,4R)-5-(9H-Fluoren-9-ylmethoxycarbonylamino)-proline-1,2,4-tricarboxylic acid 1-benzyl ester 2-*tert*-butyl ester (2.0 g, 3.4 mmol). $[\alpha]^{23}_{D}$ = -3.0° (*c* 1.0, $CHCl_3$); IR (film) ν_{max} 3313, 2978, 1710, 1525, 1450, 1419, 1356, 1258, 1156, 1109, 961, 831, 758, 741, 697; ^{1}H NMR (300 MHz, 77°C, DMSO-*d*6) δ 8.02 (br s, 1H), δ 7.86 (d, 7.5 Hz, 2H), δ 7.68 (d, 3.6 Hz, 7.5 Hz, 2H), δ 7.30-7.45 (m, 9H), δ 6.42 (tt, 5.1 Hz, 52.2 Hz, 1H), δ 5.11 (br s, 2H), δ 4.60 (t, 13.8 Hz, 2H), δ 4.31-4.47 (m, 3H), δ 4.22 (t, 6.3 Hz, 1H), δ 4.08 (d, 11.4 Hz, 1H), δ 3.67 (d, 11.4 Hz, 1H), δ 2.87 (br m, 1H), δ 2.35 (br d, 8.7 Hz), δ 1.38 (br s, 9H); ^{13}C NMR (300 MHz, 22°C, DMSO-*d*6) δ 170.8, δ 170.3, δ 155.8, δ 154.0, δ 144.1, δ 141.2, δ 137.0, δ 128.3, δ 128.2, δ 127.8, δ 127.7, δ 127.6, δ 127.5, δ 127.3, δ 127.2, δ 127.0, δ 125.6, δ 120.5, δ 114.6, δ 111.6 & 109.7 & 107.7, δ 81.6, δ 66.8, δ 63.6 & 62.7, δ 60.9 & 60.6 (rotamers), δ 58.8 & 58.4 (rotamers), δ 55.0 & 54.6 (rotamers), δ 47.0, δ 38.9 & δ 37.8 (rotamers), δ 27.9, δ 27.8; HRMS-ES (*m/z*): 723.2319 ($C_{36}H_{36}N_2O_8F_4$ + Na^+ requires 723.2305).

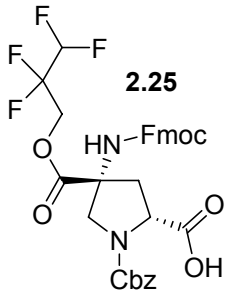

(2*R*,4*R*)-5-(9H-Fluoren-9-ylmethoxycarbonylamino)-proline-1,2,4-tricarboxylic acid 1-benzyl ester 4-(2,2,3,3 tetrafluoro) propyl ester (2.25)

The general procedure for the synthesis of compound **2.16** was followed for the synthesis of **2.25** (1.1 g, 94% yield) starting with compound **2.24** (1.3 g, 1.9 mmol). $[\alpha]^{23}_{D} = 22.7°$ (*c* 1.0, $CHCl_3$); IR (film) ν_{max} 3304, 3034, 1716, 1521, 1419, 1260, 1109, 741, 697; ^{1}H NMR (300 MHz, 77°C, DMSO-*d*6) δ 8.08 (br s, 1H), δ 7.86 (d, 7.5 Hz, 2H), δ 7.67 (d, 7.5 Hz, 2H), δ 7.30-7.44 (m, 9H), δ 6.41 (tt, 5.1 hz, 52.2 Hz, 1H), δ 5.10 (br s, 2H), δ 4.58 (t, 14.1 Hz, 2H), δ 4.34-4.39 (m, 3H), δ 4.11-4.25 (m, 2H), δ 3.59 (d, 11.7 Hz, 1H), δ 2.87 (br m, 1H), δ 2.31 (br dd, 6.3 Hz, 13.5 Hz, 1H); ^{13}C NMR (300 MHz, 22°C, DMSO-*d*6) δ 173.2, δ 172.8, δ 171.0, δ 156.4, δ 154.1 & 153.9, δ 144.1, δ 141.2, δ 137.1, δ 128.9, δ 128.8, δ 128.4, δ 128.2, δ 128.0, δ 127.6, δ 127.5, δ 125.6, δ 120.6, δ 114.8, δ 109.6, δ 66.9, δ 66.4, δ 63.4, δ 62.6 & 61.0 (rotamers), δ 60.8, δ 58.1 & 57.8 (rotamers), δ 55.2 & 54.8 (rotamers), δ 47.0, δ 39.1 & δ 38.0 (rotamers); HRMS-ES (*m/z*): 667.1699 ($C_{32}H_{28}N_2O_8F_4 + Na^+$ requires 667.1679).

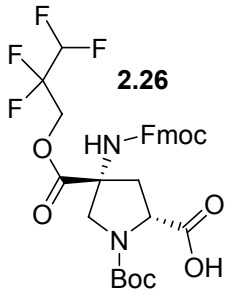

(2*R*,4*R*)-5-(9H-Fluoren-9-ylmethoxycarbonylamino)-proline-1,2,4-tricarboxylic acid 1-*tert*-butyl ester 4-(2,2,3,3 tetrafluoro) propyl ester (2.26)

Compound **2.25** (1.0 g, 1.6 mmol) was dissolved in dry THF (30 mL) and transferred to a 100 mL round bottom flask. To the solution were added 10 wt % Pd/C (.1 g, 10% by wt **2.25**) and di-*tert*-butyl dicarbonate (.85 g, 3.9 mmol). The solution was degassed by vacuum filtration and backfilled with H_2 via a balloon (cycle repeated 3 times). The reaction progress was monitored via HPLC. The reaction was complete after 24 hours. The solution was filtered through fluted filter paper, and the residual Pd/C washed repeatedly with $CHCl_3$. The solution was concentrated by rotary evaporation and adsorbed onto celite. This was followed by immediate purification by flash chromatography on a Combiflash companion purification system (40g silica comlumn, 0-10% MeOH/$CHCl_3$ gradient). All pure fractions were combined, and the solvent removed by rotary evaporation and under reduced pressure overnight yielding a white foamy solid **2.26** (.85 g, 90 % yield). $[\alpha]^{23}_D$ = 51.0° (*c* 1.0, $CHCl_3$); IR (film) ν_{max} 3304, 2979, 1699, 1530, 1478, 1451, 1409, 1369, 1259, 1109, 830, 759, 742; ^{1}H NMR (300 MHz, 22°C, DMSO-*d*6) ; δ 8.44 (s, 1H), δ 7.89 (d, 4.5 Hz, 2H), δ 7.70 (d, 4.5 Hz, 2H), δ 7.31-7.43 (m, 4H), δ 6.35-6.60 (m, 1H), δ 4.63 (t, 8.1 Hz, 2H), δ 4.28-4.32 (m, 2H), δ 4.21 (t, 4.2 Hz, 1H), δ 4.17 (t, 4.5 Hz, 1H), δ 4.08 (rotamer, d, 1H), δ 4.01 (rotamer, d, 1H), δ 3.42-3.45 (rotamers, 2H), δ 2.76-2.87 (rotamer, 1H), δ 2.19-2.29 (rotamer, 1H), δ 1.35-1.40 (rotamer, 9H); ^{13}C NMR (300 MHz, 22°C,

DMSO-*d*6) δ 174.0, δ 171.0, δ 156.4, δ 153.6, δ 144.1, δ 141.2, δ 128.4, δ 127.6, δ 125.6, δ 120.6, δ 114.8, δ109.6, δ 79.7 & 79.1, δ 66.4, δ 63.2 & 62.5 (rotamers), δ 60.7, δ 58.4 & 58.1 (rotamers), δ 55.1 & 54.7 (rotamers), δ 47.0, δ 38.4 & δ 37.9 (rotamers); HRMS-ES (*m/z*): 633.1822 ($C_{29}H_{30}N_2O_8F_4$ + Na^+ requires 633.1836).

5.2 CHAPTER 3

General: Solid phase chemistry was carried out using a home-made solid phase peptide synthesizer. Anhydrous DMF used in coupling reactions was purchased from Aldrich Chemical Company. Dry CH_2Cl_2 was distilled from CaH_2 and used for coupling reactions. Diisopropylethyl amine (DIPEA) was distilled under N_2 first from ninnydrin and secondly from KOH and stored over molecular sieves (4A). O-(7-azabenzotriazol-1-yl)-N,N,N',N'-tetramethyluronium hexafluorophosphate (HATU) was purchased from Aldrich or GenScript Coorporation. 1-(mesitylene-2-sulfonyl)-3-nitro-1,2,4-triazole was purchased from Acros. The hydroxymethyl polystyrene resin was purchased from NovaBiochem. N-α-Fmoc-O-t-butyl-L-tyrosine was purchased from NovaBiochem. The Pf1 bacteriophage was purchased from Asla Biotech. All other reagents were purchased from Aldrich or Acros and used as received. All solid phase reactions were mixed by agitation with bubbling argon thus maintaining a constant argon atmosphere. HPLC-MS analysis was performed on a Hewlett-Packard Series 1050 instrument with a diode array detector, HP 1100 MS detector (ESI), using a Waters Xterra MS C_{18} column (3.5 μm packing, 4.6 X 100 mm). Purification by preparative HPLC was performed on a Varian Prostar 500 HPLC system with a Waters Xterra MS C_{18} column (5 μm packing, 30 X 100 mm) or a Waters Xterra MS C_{18} column (5 μm packing, 10 x 100 mm). NMR

experiments were performed on Bruker Advance DRX 600 MHz spectrometer or a Bruker Advance DRX 700 MHz with a cryoprobe. Chemical shifts are reported relative to a (trimethylsilyl)propionic-2,2,3,3-d_4 acid. ^{1}H and ^{13}C assignment was carried out with Sparky 3, T. D. Goddard and D.G. Kneller, University of California, San Francisco. REDCAT was used for analysis of the residual dipolar coupling values and ACME used for $^{3}J_{HH}$ coupling extraction.

Synthesis of *pip5(2S5R)-pip5(2R5S)-pro4(2S4S)-(L)-tyrosine*

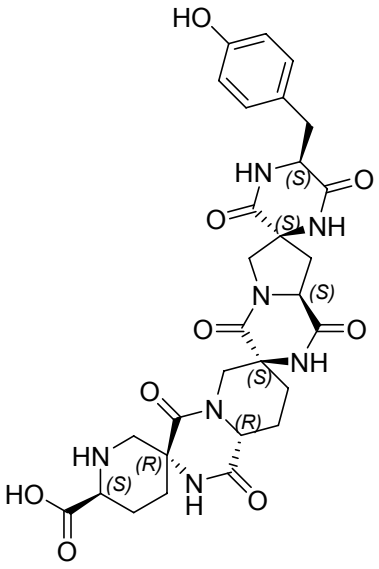

3.1

To a 10 mL polypropylene solid phase peptide synthesis (SPPS) reaction vessel was added hydroxymethyl polystyrene resin (30 mg, 0.98 mmol/g substitution). The resin was swelled in DCM for 1 hour. In a 2 mL polypropylene micro centrifuge vial *pip5(2S5R)* Boc-monomer (91.8 mg, 147 μmol) was dissolved in dry DCM (588 μL) and MeIm (8.8 μL, 111 μmol) was added. To this solution was added MSNT (43.6 mg, 147 μmol). The resulting solution was transferred to the SPPS reaction vessel and was mixed with gently bubbling argon for 1 hour.

This procedure was repeated. The resin was washed repeatedly with DCM and IPA and then DMF and MeOH to assure the removal of residual reactants. The resin was swelled in DMF for ten minutes. The terminal Fmoc protecting group was removed with 20% piperidine in DMF for 30 minutes and analysis by UV-Vis of the piperidine-dibenzofulvene adduct (λ_{max}=301 nm, ε = 7800 $M^{-1}cm^{-1}$) indicated near quantitative coupling to the resin. The remaining *pip5(2R5S)* Boc-monomer, *pro4(2S4S)* Boc-monomer, and N-α-Fmoc-O-t-butyl-L-tyrosine were coupled sequentially to the resin (2 eq. of N-Fmoc protected monomer, 2 eq. of HATU, 4 eq. of DIPEA, 0.2 M in 20%DCM/DMF, 30 minute reaction time). Every monomer coupling was repeated once as to insure complete coupling. After the double couplings the resin was washed with DMF and then capped with a 400:100:8 DMF:Ac_2O:DIPEA solution for ten minutes. The terminal Fmoc protecting group was removed with 20% piperidine in DMF for 30 minutes and UV-Vis spectroscopic analysis of the piperidine-dibenzofulvene adduct (λ_{max}=301 nm, ε = 7800 $M^{-1}cm^{-1}$) was used to quantitate overall couplings. After the removal of the last terminal Fmoc group, the resin was swelled in DCM and treated twice with 50% TFA/DCM for 30 minutes to remove the Boc protecting groups on all secondary amines. The resin was neutralized with 10% TEA/DCM and washed repeatedly with DCM and MeOH. Residual solvent was removed under reduced pressure. The dry resin beads were transferred to a 10 mL microwave reaction vessel fitted with a stir bar. 5 mL of a solution of 100 mM AcOH and 50 mM Et_3N in o-xylene was added, and the vessel was capped and placed in a microwave reactor (CEM Discover) and irradiated (300 W max power, 130 °C, 5 min ramp) with continuous stirring for 30 minutes. The resin was then transferred to a 10 mL SPPS polypropylene reactor and washed repeatedly with DCM and MeOH. Residual solvent was removed under reduced pressure. To the dry resin was added 1 mL TFA, 60 μL thioanisole, and 30 μL EDT. The solution was cooled in an ice bath while being

stirred. To the cleavage solution was added 60 μL TFMSA, and the resulting solution was stirred vigorously for 3 hours. The product was precipitated in 40 mL of anhydrous diethyl ether while stirring. The resulting precipitate was pelleted by centrifugation, and the ether decanted. The pellet was dissolved in 1:1 H_2O/MeCN (1 mL) and purified by preparative HPLC. The desired fractions were pulled together and concentrated by freeze-drying.

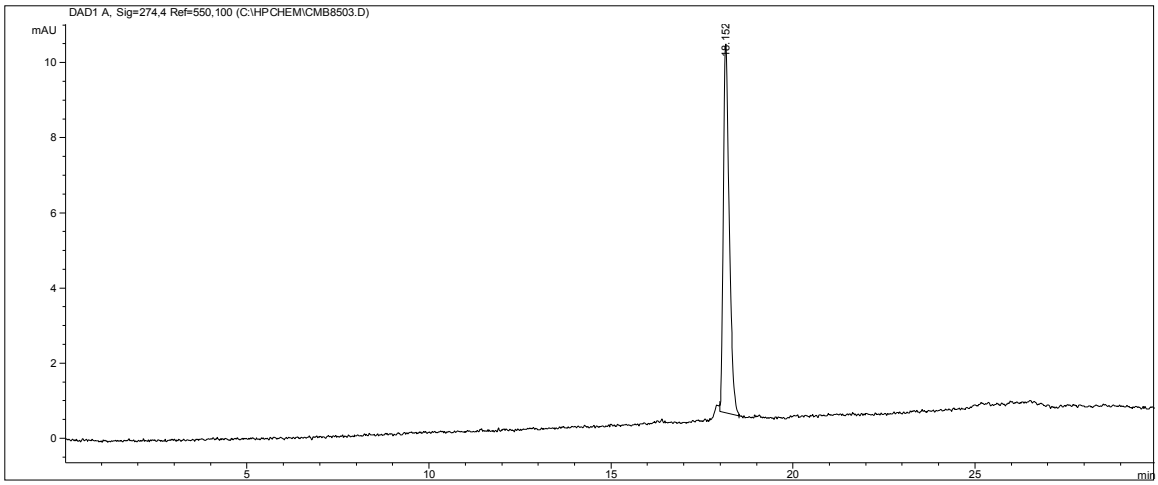

HPLC-MS: column, Waters XTerra MS C_{18} column; mobile phase , MeCN/water (0.1% formic acid), 0% to 25% MeCN over 30 minutes; flow rate, 0.4 mL/min; UV detection at 274 nm; t_R 18.152 min; ES-MS m/z (ion) 624.2 ($M+H^+$).

2-D NMR experiments on 3.1

^1H, HMBC, and TOCSY NMR experiments on a 5 mM solution of **3.1** and HSQC-F1 dimension no decoupling and ROESY NMR experiments on a 11 mM solution of **3.1** in 90% H_2O/D_2O with 20 mM acetate buffer at pH 3.4. Software package Sparky was used to assign the oligomer.

Phase-Sensitive COSY

A phase-sensitive COSY with States acquisition mode (256 data points in F1 and 4K data points in the F2 dimension zero filed back to 4K for a resolution of 1.36 Hz/point) was acquired on a 7.0 mM solution of **3.1** in D_2O with 40 mM phosphate buffer at pH 7.5. Using the software package ACME, the $^3J_{HH}$ coupling constants of each observed multipet were extracted.

Preparation of unaligned NMR sample and HSQC acquisition

A 6.66 mM solution of **3.1** (2.00 umoles) was prepared in 40 mM phosphate buffer (300 μL) at a pH of 7.5. The solution was added to a Shigemi tube with an elongated glass pipette. An HSQC with the 180 ° pulse on the ^1H channel during the t1 evolution period and decoupling during signal acquisition eliminated was acquired with 4k data points in the F1 dimension zero filed back to 4k and 4k data points in the F2 dimension.

Preparation of Pf1 phage stock solution

150 μL of a Pf1 magnetic resonance co-solvent was added to a 15 mL Biomax filter with a 10 NMWL membrane. To this was added 1 mL of D_2O followed by rapid mixing with a disposable pipette. The sample was spun down at 3200 rpm at 4 C° for 2 hours. Subsequently, another 1 mL of D_2O was added followed my mixing. The sample was spun down once again at 3200 rpm at 4 C° for 4.5 hours. To this concentrated Pf1 solution was added 200 μL of 40 mM phosphate buffer at pH 7.5. The concentration of Pf1 solution was determined to be 26.33 mg/mL by UV-VIS absorbance (270 nm, 2.25 $mL*mg^{-1}*cm^{-1}$).

Preparation of Pf1 aligned NMR sample and HSQC acquisition

To the above 6.66 mM solution of **3.1** in 300 μL of 40mM phosphate buffer at pH 7.5 was added 183.7 μL of the prepared Pf1 phage stock solution (26.33 mg/mL) to create a 10mg/mL phage sample in the now 4.14 mM sample of **3.1**. An HSQC with the 180 ° pulse on the ^{1}H channel during the t1 evolution period and decoupling during signal acquisition eliminated was acquired with 4k data points in the F1dimension zero filed back to 4k and 2k data points in the F2 dimension.

5.3 CHAPTER 4

General: Solid phase chemistry was carried out using a home-made solid phase peptide synthesizer. Anhydrous DMF used in coupling reactions was purchased from Aldrich Chemical Company. Dry CH_2Cl_2 was distilled from CaH_2 and used for coupling reactions. Diisopropylethyl amine (DIPEA) was distilled under N_2 first from ninnydrin and secondly from KOH and stored over molecular sieves (4A). O-(7-azabenzotriazol-1-yl)-N,N,N',N'-tetramethyluronium hexafluorophosphate (HATU) was purchased from Aldrich or GenScript Coorporation. The dansyl novatag resin was purchased from NovaBiochem. N-α-Fmoc-N-γ-1-(4,4-dimethyl-2,6-dioxocyclohex-1-ylidene)-3-methylbutyl-L-diaminobutanoic acid, N-α-Fmoc-N-δ-4-methyltrityl-L-ornithine, and N-α-Fmoc-N-ε-4-methyltrityl-L-diaminoproprionic acid were purchases from NovaBiochem. (S)-N-Fmoc-1-naphthylalanine was purchased from Acros. The 3-carboxy-2-fluorophenylboronic acid was purchased from AsymChem. All other reagents were purchased from Aldrich or Acros and used as received. All solid phase reactions were mixed by agitation with bubbling argon thus maintaining a constant argon atmosphere. HPLC-

MS analysis was performed on a Hewlett-Packard Series 1050 instrument with a diode array detector, HP 1100 MS detector (ESI), using a Waters Xterra MS C_{18} column (3.5 μm packing, 4.6 X 100 mm). Purification by preparative HPLC was performed on a Varian Prostar 500 HPLC system with a Waters Xterra MS C_{18} column (5 μm packing, 30 X 100 mm) or a Waters Xterra MS C_{18} column (5 μm packing, 10 x 100 mm). Fluorescence excitation spectra were obtained on a Cary Eclipse Fluorescence spectrophotometer.

Synthesis of 2-fluoro-3-(4,4,5,5-tetramethyl-1,3,2-dioxaborolan-2-yl)benzoic acid (4.1)

The 3-carboxy-2-fluorophenylboronic acid (63 mg, 0.33 mmol) was transferred to a 25 mL round bottom flask. To the same round bottom flask was added pinacol (39.4 mg, 0.33 mmol). The solids were suspended in a 1:1 mixture of toluene/THF (8 mL). The solvent was removed under reduced pressure by rotary evaporation (20 C°) to yield a white powder. The process of solvent evaporation was repeated three times to yield **4.1** in quantitative amounts. The product was not purified and was used as generated.

^{1}H NMR (300 MHz, 77 °C, DMSO-*d*6) δ 7.95 (br t, 1H), δ 7.80 (br t, 1H), δ 7.28 (t, 7.14 Hz, 1H), δ 1.28 (s, 12H); ^{13}C NMR (75.4 MHz, 20 °C, DMSO-*d*6) δ 167.09, δ 165.64, δ 163.62, δ141.15, δ135.66, δ 124.56, δ 120.10, δ 84.41, δ 25.07.

Synthesis of Glucose Actuator Molecule (4.3)

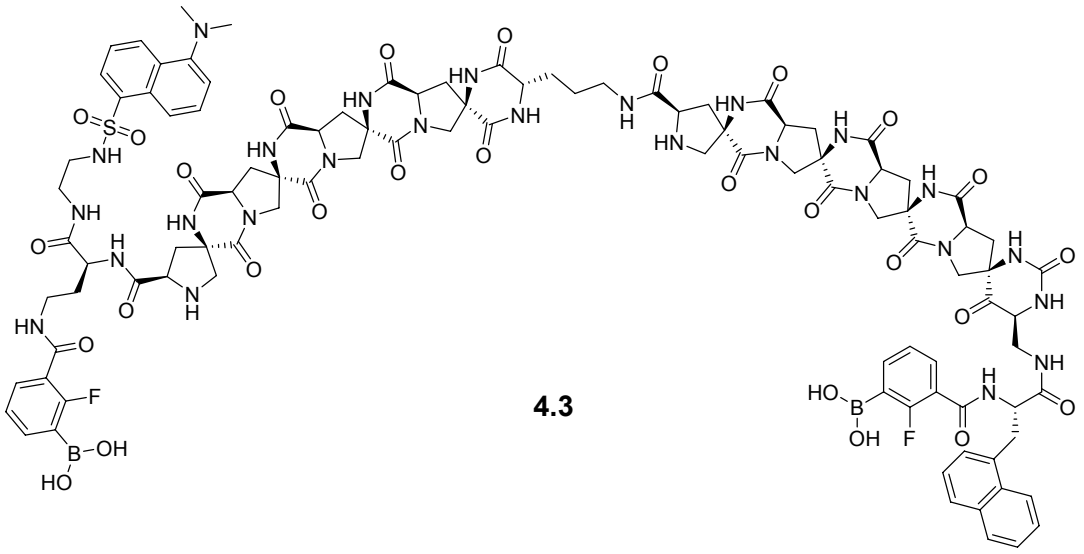

4.3

To a 10 mL polypropylene solid phase peptide synthesis (SPPS) reaction vessel was added dansyl novatag resin (25 mg, 0.51 mmol/g substitution). The resin was swelled in DMF for 1 hour followed by deprotection of the terminal Fmoc protecting group with 20% piperidine in DMF for 30 minutes. In a 2 mL polypropylene micro centrifuge vial N-α-Fmoc-N-γ-1-(4,4-dimethyl-2,6-dioxocyclohex-1-ylidene)-3-methylbutyl-L-diaminobutanoic acid (25.5 μmol) and HATU (25.5 μmol) (2 eq. of N-Fmoc protected acid, 2 eq. of HATU) were dissolved in 20%DMF/DCM (127 μL). To this was added DIPEA (4 eq). The resulting solution was transferred to the SPPS reaction vessel and was mixed with gently bubbling argon for 30 min. This coupling procedure was repeated. The resin was washed with DMF and then capped with a 400:100:8 DMF:Ac_2O:DIPEA solution for 10 minutes. The terminal Fmoc protecting group was removed with 20% piperidine in DMF for 30 minutes and UV-Vis spectroscopic analysis of the piperidine-dibenzofulvene adduct (λ_{max}=301 nm, ε = 7800 $M^{-1}cm^{-1}$) indicated quantitative coupling. The resin was subsequently washed with DMF and IPA and then swelled in DMF for

10 minutes. Next the *pro4(2R4R)* Boc-monomer, *pro4(2R4R)* Boc-monomer, *pro4(2R4R)* Boc-monomer, *pro4(2R4R)* Boc-monomer, and N-α-Fmoc-N-δ-4-methyltrityl-L-ornithine were coupled sequentially to the resin (2 eq. of N-Fmoc protected acid, 2 eq. of HATU, 4 eq. of DIPEA, 0.2 M in 20%DCM/DMF, 30 minute reaction time). Every coupling was repeated once as to insure complete coupling. After the double couplings the resin was washed with DMF and then capped with a 400:100:8 DMF:Ac_2O:DIPEA solution for 10 minutes. The terminal Fmoc protecting group was removed with 20% piperidine in DMF for 30 minutes except that of the N-α-Fmoc-N-δ-4-methyltrityl-L-ornithine which was removed for 2 hours in order to insure complete DKP closure between residues. The resin was washed with DMF and IPA repeatedly and then DCM and MeOH followed by swelling in DCM. The resin was treated with 1% TFA/DCM for two minutes for a repetition of 10 times. After washing with DCM and MeOH, DMF and IPA, and swelling in DMF for 10 mintues; the *pro4(2R4R)* Boc-monomer, *pro4(2R4R)* Boc-monomer, *pro4(2R4R)* Boc-monomer, *pro4(2R4R)* Boc-monomer, and N-α-Fmoc-N-ε-4-methyltrityl-L-diaminoproprionic acid were coupled sequentially to the resin (2 eq. of N-Fmoc protected acid, 2 eq. of HATU, 4 eq. of DIPEA, 0.2 M in 20%DCM/DMF, 30 minute reaction time). Every coupling was repeated once as to insure complete coupling. After the double couplings the resin was washed with DMF and then capped with a 400:100:8 DMF:Ac_2O:DIPEA solution for 10 minutes. The terminal Fmoc protecting group was removed with 20% piperidine in DMF for 30 minutes except that of the N-α-Fmoc-N-ε-4-methyltrityl-L-diaminoproprionic acid which was removed for 2 hours in order to insure complete DKP closure between residues. The resin was washed with DMF and IPA repeatedly and then DCM and MeOH followed by swelling in DCM. The resin was treated with 1% TFA/DCM for two minutes for a repetition of 10 times. After washing with DCM and MeOH, DMF and IPA, and swelling in DMF for 10

mintues; the remaining (S)-N-Fmoc-1-naphthylalanine was coupled (2 eq. of N-Fmoc protected acid, 2 eq. of HATU, 4 eq. of DIPEA, 0.2 M in 20%DCM/DMF, 30 minute reaction time) as done in previous couplings. The terminal Fmoc protecting group was removed by treatment with 20% piperidine in DMF for 30 minutes.

Removal of ivDde protecting group from Dab residue

A 10 mol solution of 4.5:1:4 Allyl alcohol:hydrazine:DMF was made. The resin was swelled in DMF prior to treatment and was treated with 1 mL of this solution 10 times for 3 minutes each treatment. The resin was then subsequently washed with DMF and IPA and then swelled in DMF for 10 minutes.

Coupling of Pinacol Boronate 4.1

To the remaining two free amines of the scaffold was coupled the pinacol boronate (5 eq to 25 mg resin, 5 eq. of HATU, 10 eq. of DIPEA, 0.2 M in 20%DCM/DMF, 1 hour reaction time). The coupling was repeated five times to insure complete coupling to the free primary and secondary amine. The resin was then washed thoroughly with DMF and IPA and subsequently swelled in DMF for 10 minutes.

Deprotection of Pinacol Boronate

To the resin was added 1 mL of 10% N-methyl-diethanolamine in DMF and was mixed with agitation by bubbling argon. The solution was drained and refilled every 20 minutes for 2 hours. The resin was then washed with DMF. Next was added 1 mL of 10% 2M HCl in DMF and was mixed with agitation by bubbling argon. The solution was drained and refilled every 15 minutes

for 2 hours. The resin was subsequently washed repeatedly with DMF and IPA followed by DCM and MeOH. Residual solvent was removed under reduced pressure.

Cleavage of Scaffold from Resin

To the dry resin was added 600 μL of a 95% TFA, 2,5% TIPS, and 2.5% H_2O solution. The SPPS reactor was fitted with a stir bar and was stirred for 3 hours. After this time, the cleavage solution was dripped into a 15 mL Falcon tube. The TFA was evaporated under a constant stream of N_2. The remaining residue was dissolved in 1.6 mL of extra dry NMP, transferred to a HPLC glass vial, and was analyzed by HPLC-MS.

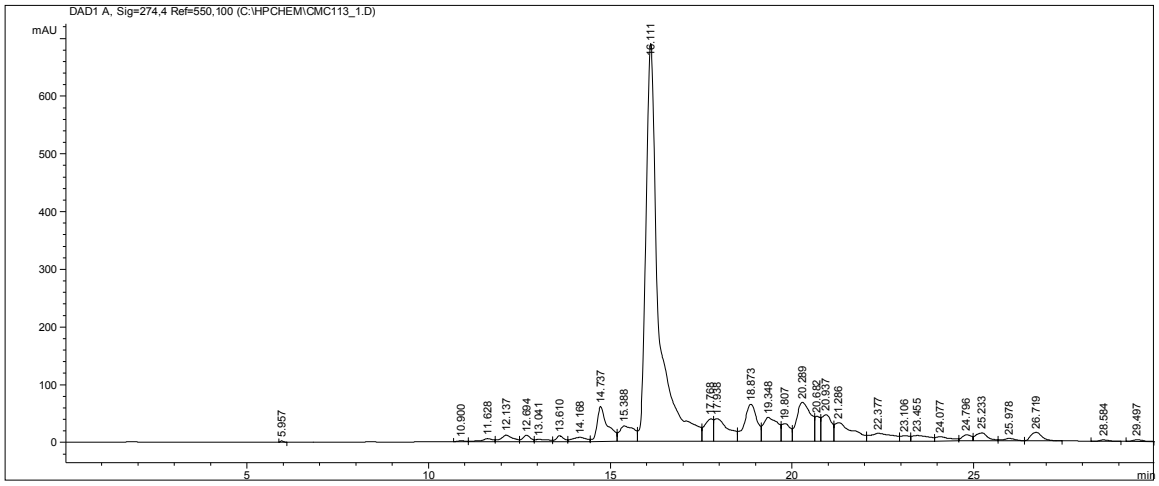

HPLC-MS: column, Waters XTerra MS C_{18} column; mobile phase , MeCN/water (0.1% formic acid), 5% to 50% MeCN over 30 minutes; flow rate, 0.4 mL/min; UV detection at 274 nm; t_R 16.111 min; ES-MS m/z (ion) 1210 ($M+2H^+$); m/z ion 807.5 ($M+3H^+$); m/z ion 605.8 ($M+4H^+$).

To the NMP solution of cleaved product was added 400 μL of redistilled piperidine. The solution was stirred under nitrogen overnight. The DKP closure was found to be complete and the product was precipitated in 35 mL of cold ether. The precipitate was pelleted by

centrifugation and was purified by preparative HPLC. The desired fractions were pulled together and concentrated by freeze-drying.

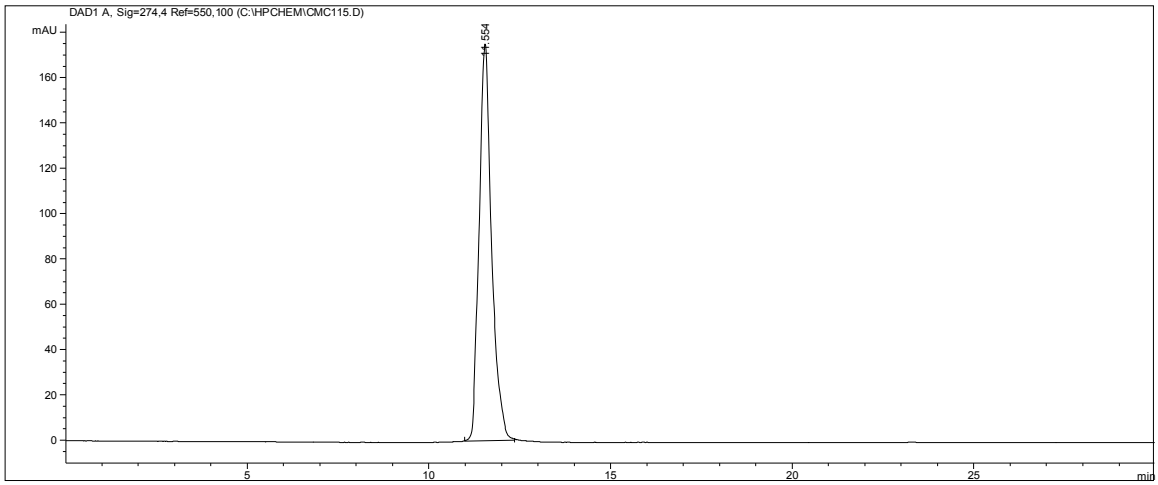

HPLC-MS: column, Waters XTerra MS C_{18} column; mobile phase , MeCN/water (0.1% formic acid), 5% to 95% MeCN over 30 minutes; flow rate, 0.4 mL/min; UV detection at 274 nm; t_R 11.554 min; ES-MS m/z (ion) 1114.5 ($M+2H^+$); m/z ion 743.5 ($M+3H^+$).

General Procedure: Saccharide Fluorescence Titrations

Fluorescence excitation spectra were obtained on a Cary Eclipse Fluorescence spectrophotometer. The excitation and emission slits were set to 5 nm. Emission was monitored at 520 nm and samples irradiated between 270 and 450 nm at a scan rate of 120 nm/min. Samples were measured in a 1 cm quartz cell (NSG Precision Cells, Inc.). The concentration of glucose sensor was determined to be 10 μM for each titration in 0.1 M phosphate buffer at pH 7.4. The saccharide was added as a small concentrated solution (ranging from 0-100 mmol). Each titrated sample was scanned five times sequentially, and these five scans were averaged. The excitation spectra were normalized so that the emission maximum of the dansyl group (337 nm) was 100 units for all samples.

NMR titration of 3-carboxy-2-fluorophenyl boronic acid with glucose

^{1}H NMR experiments were performed on a Bruker Advance 300 MHz NMR. Upon addition of glucose to a solution of 3-carboxy-2-fluorophenyl boronic acid in H_2O, the chemical shifts of the aromatic protons are shifted upfield. The reversible binding between the boronic acid and glucose is slower than the NMR timescale giving rise to the occurrence of two sets of aromatic proton peaks.

A total of 9 samples of 3-carboxy-2-fluorophenyl boronic acid and glucose were made. Each NMR sample contained a total concentration of 5.4 mM of 3-carboxy-2-fluorophenyl boronic acid in D_2O phosphate buffer at a pH of 7.4. Each NMR sample contained a different concentration of glucose (21.7 mM, 43.5 mM, 65.2 mM, 87.0 mM, 108.4 mM, 163.0 mM, 217.4 mM, 271.1 mM, and 380.4 mM).

The particular proton resonance monitored in this study was δ 7.13. The new proton resonance that was generated from the glucose bond boronic acid was δ 6.99. These peaks were integrated from each NMR sample listed above. The integral ratio between the two different resonances were plotted vs. the ln[glucose concentration].

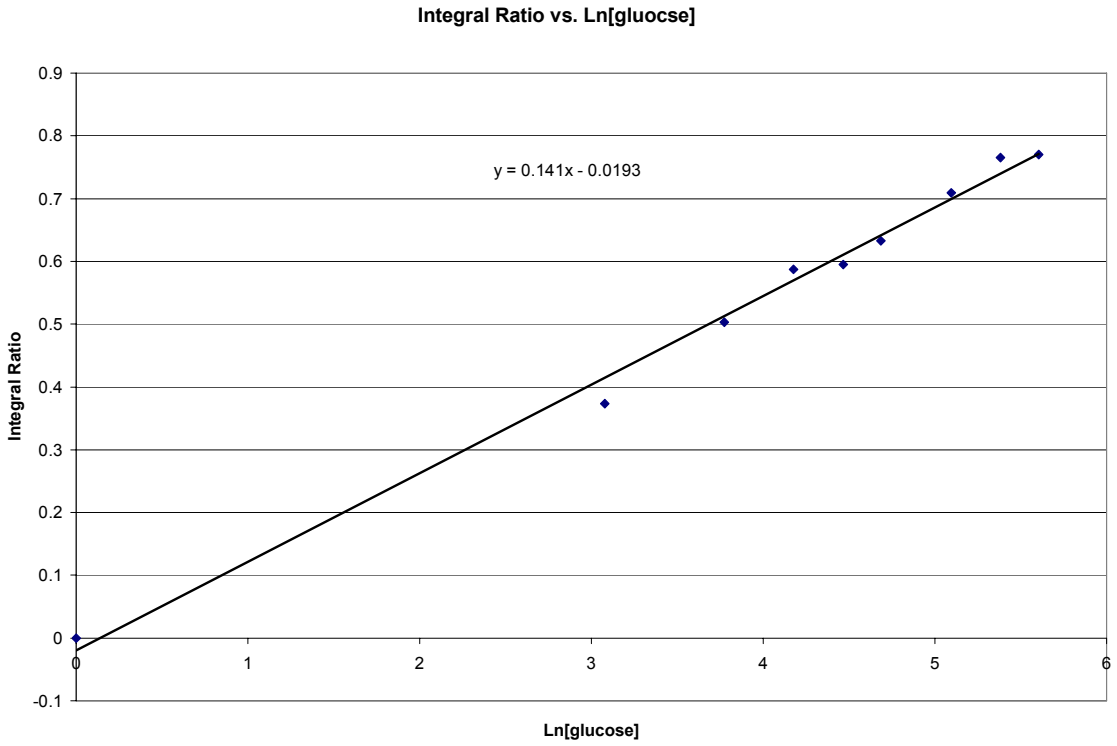

The K_d occurs at when the boronic acid is half-bound to glucose. Using equation y=0.141ln(x) – 0.0193 and substituting 0.5 for y, the K_d was deteremined to be ~40 mM.

.

BIBLIOGRAPHY

(1) Roco, M. C. a. B., W.S. *Journal of the Nanoparticle Research* 2005, 1-13.

(2) http://www.nano.gov/html/facts/whatIsNano.html.

(3) Petitjean, A.; Khoury, R. G.; Kyritsakas, N.; Lehn, J.-M. *Journal of the American Chemical Society* 2004, *126*, 6637-6647.

(4) Nielsen, K. A.; Cho, W.-S.; Jeppesen, J. O.; Lynch, V. M.; Becher, J.; Sessler, J. L. *Journal of the American Chemical Society* 2004, *126*, 16296-16297.

(5) Flood, A. H.; Stoddardt, J. F.; Steuerman, D. W.; Heath, J. R. *Science (Washington, DC, United States)* 2004, *306*, 2055-2056.

(6) Nguyen, T. D.; Leung, K. C. F.; Liong, M.; Pentecost, C. D.; Stoddart, J. F.; Zink, J. I. *Organic Letters* 2006, *8*, 3363-3366.

(7) Liu, N.; Dunphy, D. R.; Atanassov, P.; Bunge, S. D.; Chen, Z.; Lopez, G. P.; Boyle, T. J.; Brinker, C. J. *Nano Letters* 2004, *4*, 551-554.

(8) Kaszynski, P.; Friedli, A. C.; Michl, J. *Journal of the American Chemical Society* 1992, *114*, 601-20.

(9) Moore, J. S. *Accounts of Chemical Research* 1997, *30*, 402-413.

(10) Zhao, D.; Moore, J. S. *Chemical Communications (Cambridge, United Kingdom)* 2003, 807-818.

(11) Heemstra, J. M.; Moore, J. S. *Organic Letters* 2004, *6*, 659-662.

(12) Appella, D. H.; Barchi, J. J., Jr.; Durell, S. R.; Gellman, S. H. *Journal of the American Chemical Society* 1999, *121*, 2309-2310.

(13) Fisk, J. D.; Gellman, S. H. *Journal of the American Chemical Society* 2001, *123*, 343-344.

(14) Chung, Y. J.; Huck, B. R.; Christianson, L. A.; Stanger, H. E.; Krauthauser, S.; Powell, D. R.; Gellman, S. H. *Journal of the American Chemical Society* 2000, *122*, 3995-4004.

(15) English, E. P.; Chumanov, R. S.; Gellman, S. H.; Compton, T. *Journal of Biological Chemistry* 2006, *281*, 2661-2667.

(16) Schmitt, M. A.; Choi, S. H.; Guzei, I. A.; Gellman, S. H. *Journal of the American Chemical Society* 2006, *128*, 4538-4539.

(17) Dahiyat, B. I.; Mayo, S. L. *Science (Washington, D. C.)* 1997, *278*, 82-87.

(18) DeGrado, W. F.; Summa, C. M.; Pavone, V.; Nastri, F.; Lombardi, A. *Annual Review of Biochemistry* 1999, *68*, 779-819.

(19) Levins Christopher, G.; Schafmeister Christian, E. *Journal of the American Chemical Society* 2003, *125*, 4702-4703.

(20) Levins, C. G.; Schafmeister, C. E. *Journal of Organic Chemistry* 2005, *70*, 9002-9008.

(21) Levins, C. G.; Brown, Z. Z.; Schafmeister, C. E. *Organic Letters* 2006, *8*, 2807-2810.

(22) Habay, S. A.; Schafmeister, C. E. *Organic Letters* 2004, *6*, 3369-3371.

(23) Gupta, S.; Das, B. C.; Schafmeister, C. E. *Organic Letters* **2005**, *7*, 2861-2864.

(24) Pellicciari, R.; Natalini, B.; Luneia, R.; Marinozzi, M.; Roberti, M.; Rosato, G. C.; Sadeghpour, B. M.; Synyder, J. P.; Monahan, J. B.; Moroni, F. *Medicinal Chemistry Research* **1992**, *2*, 491-6.

(25) Krapcho, A. P.; Glynn, G. A.; Grenon, B. J. *Tetrahedron Letters* **1967**, 215-17.

(26) Bucherer, H. T.; Brandt, W. *Journal fuer Praktische Chemie (Leipzig)* **1934**, *140*, 129-50.

(27) Ferguson, D. M.; Raber, D. J. *Journal of the American Chemical Society* **1989**, *111*, 4371-8.

(28) Inc, C. C. G.; 2005.06 ed ed. Montreal, 2005.

(29) Halgren, T. A. *Journal of Computational Chemistry* **1996**, *17*, 490-519.

(30) Halgren, T. A. *Journal of Computational Chemistry* **1996**, *17*, 520-52.

(31) Halgren, T. A. *Journal of Computational Chemistry* **1996**, *17*, 553-86.

(32) Halgren, T. A. *Journal of Computational Chemistry* **1996**, *17*, 616-41.

(33) Halgren, T. A.; Nachbar, R. B. *Journal of Computational Chemistry* **1996**, *17*, 587-615.

(34) Kubik, S.; Meissner, R. S.; Rebek, J., Jr. *Tetrahedron Letters* **1994**, *35*, 6635-8.

(35) Gupta, S.; Macala, M.; Schafmeister, C. E. *Journal of Organic Chemistry* **2006**, *71*, 8691-8695.

(36) Sakaitani, M.; Hori, K.; Ohfune, Y. *Tetrahedron Letters* **1988**, *29*, 2983-4.

(37) Cornell, W. D.; Cieplak, P.; Bayly, C. I.; Gould, I. R.; Merz, K. M., Jr.; Ferguson, D. M.; Spellmeyer, D. C.; Fox, T.; Caldwell, J. W.; Kollman, P. A. *Journal of the American Chemical Society* **1995**, *117*, 5179-97.

(38) Yan, J.; Kline, A. D.; Mo, H.; Shapiro, M. J.; Zartler, E. R. *Journal of Organic Chemistry* **2003**, *68*, 1786-1795.

(39) Yan, J.; Zartler, E. R. *Magnetic Resonance in Chemistry* **2005**, *43*, 53-64.

(40) Mangoni, A.; Esposito, V.; Randazzo, A. *Chemical Communications (Cambridge, United Kingdom)* **2003**, 154-155.

(41) Luy, B.; Kobzar, K.; Kessler, H. *Angewandte Chemie, International Edition* **2004**, *43*, 1092-1094.

(42) Delaglio, F.; Wu, Z.; Bax, A. *Journal of Magnetic Resonance* **2001**, *149*, 276-281.

(43) Bax, A. *Protein Science* **2003**, *12*, 1-16.

(44) Losonczi, J. A.; Andrec, M.; Fischer, M. W. F.; Prestegard, J. H. *Journal of Magnetic Resonance* **1999**, *138*, 334-342.

(45) Zweckstetter, M.; Bax, A. *Journal of Biomolecular NMR* **2001**, *20*, 365-377.

(46) Valafar, H.; Prestegard, J. H. *Journal of Magnetic Resonance* **2004**, *167*, 228-241.

(47) Wang, W.; Gao, X.; Wang, B. *Current Organic Chemistry* **2002**, *6*, 1285-1317.

(48) Jiang, S.; Escobedo, J. O.; Kim, K. K.; Alptuerk, O.; Samoei, G. K.; Fakayode, S. O.; Warner, I. M.; Rusin, O.; Strongin, R. M. *Journal of the American Chemical Society* **2006**, *128*, 12221-12228.

(49) Karnati, V. V.; Gao, X.; Gao, S.; Yang, W.; Ni, W.; Sankar, S.; Wang, B. *Bioorganic & Medicinal Chemistry Letters* **2002**, *12*, 3373-3377.

(50) Gao, S.; Wang, W.; Wang, B. *Bioorganic Chemistry* **2001**, *29*, 308-320.

(51) Bielecki, M.; Eggert, H.; Norrild, J. C. *Journal of the Chemical Society, Perkin Transactions 2: Physical Organic Chemistry* **1999**, 449-456.

(52) Koschinsky, T.; Heinemann, L. *Diabetes/Metabolism Research and Reviews* **2001**, *17*, 113-123.

(53) Gerritsen, M.; Jansen, J. A.; Lutterman, J. A. *The Netherlands journal of medicine* **1999**, *54*, 167-79.

(54) Daniloff, G. Y. *Diabetes Technology & Therapeutics* **1999**, *1*, 261-266.

(55) Kerner, W. *Experimental and Clinical Endocrinology & Diabetes* **2001**, *109*, S341-S346.

(56) Atanasov, P.; Yang, S.; Salehi, C.; Ghindilis, A. L.; Wilkins, E.; Schade, D. *Biosensors & Bioelectronics* **1997**, *12*, 669-680.

(57) Norrild, J. C.; Eggert, H. *Journal of the Chemical Society, Perkin Transactions 2: Physical Organic Chemistry* **1996**, 2583-2588.

(58) James, T. D.; Sandanayake Samankumara, K. R. A.; Shinkai, S. *Angewandte Chemie, International Edition in English* **1996**, *35*, 1911-1922.

(59) Yang, W.; Gao, S.; Gao, X.; Karnati, V. V. R.; Ni, W.; Wang, B.; Hooks, W. B.; Carson, J.; Weston, B. *Bioorganic & Medicinal Chemistry Letters* **2002**, *12*, 2175-2177.

(60) Stryer, L. *Annual Review of Biochemistry* **1978**, *47*, 819-46.

(61) Schuler, B.; Lipman, E. A.; Steinbach, P. J.; Kumke, M.; Eaton, W. A. *Proceedings of the National Academy of Sciences of the United States of America* **2005**, *102*, 2754-2759.

(62) Selvin, P. R. *Nature Structural Biology* **2000**, *7*, 730-734.

(63) Haas, E.; Wilchek, M.; Katchalski-Katzir, E.; Steinberg, I. Z. *Proceedings of the National Academy of Sciences of the United States of America* **1975**, *72*, 1807-11.

(64) Springsteen, G.; Wang, B. *Tetrahedron* **2002**, *58*, 5291-5300.

(65) Mulla, H. R.; Agard, N. J.; Basu, A. *Bioorganic & Medicinal Chemistry Letters* **2004**, *14*, 25-27.

(66) Tokunaga, Y.; Ueno, H.; Shimomura, Y.; Seo, T. *Heterocycles* **2002**, *57*, 787-790.

(67) Hoeg-Jensen, T. *QSAR & Combinatorial Science* **2004**, *23*, 344-351.